



Towards optimal mixtures of working fluids: Integrated design of processes and mixtures for Organic Rankine Cycles

Journal Article

Author(s):

Schilling, Johannes ; Entrup, Marten; Hopp, Madlen; Gross, Joachim; Bardow, André 

Publication date:

2021-01

Permanent link:

<https://doi.org/10.3929/ethz-b-000438666>

Rights / license:

Creative Commons Attribution-NonCommercial-NoDerivatives 4.0 International

Originally published in:

Renewable and Sustainable Energy Reviews 135, <https://doi.org/10.1016/j.rser.2020.110179>

Towards optimal mixtures of working fluids: Integrated design of processes and mixtures for Organic Rankine Cycles

Schilling, J.^a, Entrup, M.^a, Hopp, M.^b, Gross, J.^b, Bardow, A.^{a,c,d,*}

^a*Institute of Technical Thermodynamics, RWTH Aachen University, Schinkelstraße 8,
52062 Aachen, Germany*

^b*Institute of Thermodynamics and Thermal Process Engineering, University of Stuttgart,
Pfaffenwaldring 9, 70569 Stuttgart, Germany*

^c*Institute of Energy and Climate Research - Energy Systems Engineering (IEK-10),
Forschungszentrum Jülich GmbH, Wilhelm-Johnen-Straße, 52425 Jülich, Germany*

^d*Energy and Process Systems Engineering, Department of Mechanical and Process
Engineering, ETH Zurich, Tannenstrasse 3, 8092 Zurich, Switzerland*

Abstract

Organic Rankine Cycles transform low-temperature heat from sustainable sources into electrical power. Exploiting the full potential of a low-temperature heat source requires the optimal combination of Organic Rankine Cycles and working fluid. Today, working fluids are commonly pure components. However, mixtures can significantly improve the process efficiency due to their favorable temperature-glide during evaporation and condensation. In this work, we present a method for the integrated design of Organic Rankine Cycles and working fluid mixtures, so-called 1-stage Continuous-Molecular Targeting Computer-aided mixture and blend design (CoMT-CAM^bD). In 1-stage CoMT-CAM^bD, the physically-based perturbed-chain statistical associating fluid theory (PC-SAFT) equation of state is used to model both, the equilibrium and the transport properties of the mixture. A CAM^bD formulation enables us to consider the molecular structure of the mixture components as well as its composition as de-

*Corresponding author

Email address: abardow@ethz.ch (Bardow, A.)

degrees of freedom during process optimization. A detailed sizing of the equipment allows us to optimize not only thermodynamic but also economic objectives. 1-stage CoMT-CAM^bD is demonstrated for the design of an Organic Rankine Cycle for waste heat recovery. The method identifies the optimal working fluid mixture from several million possible mixtures jointly with the corresponding optimal process and equipment, e.g., the mixture propane/diethyl ether maximizing the net power output ($P_{\text{net}} = 295 \text{ kW}$) or propene/propionaldehyde minimizing the specific investment cost ($\text{SIC} = 3,479 \text{ €/kW}$). The presented method allows us to rigorously analyze the potential of optimal mixtures compared to pure components for varying heat source and cooling medium of the process and systematically exploit the potential of working fluid mixtures for Organic Rankine Cycles.

Highlights:

- Integration of mixture design into ORC process design.
- Selection of the optimal mixture from over 42 million mixtures.
- Thermodynamic and thermo-economic assessment in a single optimization.
- Rigorous performance analysis: optimal mixtures vs. optimal pure components.
- Mixtures greatly improve the thermodynamics, economics only slightly.

Keywords: CoMT-CAMD, computer-aided mixture design, PC-SAFT, Organic Rankine Cycle

Word count: ca. 9900 words

Nomenclature

Abbreviations

CAMD	computer-aided molecular design
CAM ^b D	computer-aided mixture and blend design
CEPCI	Chemical Engineering Plant Cost Index
CoMT	continuous-molecular targeting
DICOPT	discrete and continuous optimizer
EoS	equation of state
GAMS	General Algebraic Modeling System
GC	group contribution
MILP	mixed-integer linear program
MINLP	mixed-integer nonlinear program
NLP	nonlinear program
ORC	Organic Rankine Cycle
(PC)-SAFT	(perturbed-chain) statistical associating fluid theory
QSPR	quantitative structure-property relationships
SNOPT	sparse nonlinear optimizer

Latin symbols

A	area (m ²)
A - D	scaling factors of the polynomial (generic)
c	CAM ^b D constraints (-)
c_p	molar heat capacity (J mol ⁻¹ K ⁻¹)
d	model parameter (generic)
f	objective function (generic)
F_1/F_2	constituting equations for CAMD (-)
g_1/g_2	equipment constraints (-)
h	molar enthalpy (J mol ⁻¹)
k	thermodynamic transport model (-)
$k_{i,j}$	binary interaction parameter (-)
m	segment number (-)
\dot{m}	mass flow rate (kg s ⁻¹)
M	molar mass (g mol ⁻¹)
n	number (-)
p	pressure (Pa)
P	power (W)
p_1/p_2	process constraints (-)
PEC	purchased-equipment cost (€)
s	molar entropy (J mol ⁻¹ K ⁻¹)
SIC	specific investment cost (€/kW)
t	thermodynamic equilibrium model (-)
T	temperature (K)
TCI	total capital investment (€)
x	process degrees of freedom (generic)
y^S	molecular structure (-)
z	parameters of the thermodynamic model (generic)

Greek symbols

Δ	difference (-)
ϵ/k	segment dispersion energy (K)
η	efficiency (-)
η	dynamic viscosity (Pa s)

θ	equilibrium property (generic)
κ	transport property (generic)
λ	thermal conductivity (W m ⁻¹ K ⁻¹)
μ	dipole moment (C m)
ξ	mixture composition (-)
σ	segment diameter (Å)
φ	vapor quality (-)

Subscripts

0	reference
CW	cooling water
cond	condensation
crit	critical
evap	evaporation
G	generator
glide	temperature-glide in 2-phase region
HE	heat exchanger
HS	heat source
is	isentropic
lb	lower bound
max	maximal
min	minimal
net	net value
P	pump
pure	pure component property
sh	super heating
st	turbine stage
T	turbine
ub	upper bound
wf	working fluid

Superscripts

*	reduced
Arom	aromatic
Hex	cyclohexane
id	ideal
ig	ideal gas
in	inlet
out	outlet
Pent	cyclopentane
ref	reference
red	reduced
res	residual

Sets

$i \in I$	set of mixture components
$k \in K$	set of functional groups

Constants

k_B	Boltzmann constant ($1.38 \cdot 10^{-23}$ m ² kg s ⁻² K ⁻¹)
N_A	Avogadro constant ($6.022 \cdot 10^{23}$ mol ⁻¹)

1. Introduction

A potential sustainable source for power generation is low-grade heat, e.g., geothermal heat [1], solar heat [2] or waste heat of industrial [3], automotive [4] or maritime [5] applications. To utilize these widely available resources of low-grade heat, Organic Rankine Cycles (ORC) are a promising technology [6, 7].

To ensure optimal use of a heat source, both the ORC process and its working fluid have to be optimized [8]. In ORCs, pure components are commonly used as working fluid. However, mixtures can significantly increase the performance since the evaporation and condensation temperatures continuously change due to the change in vapor/liquid composition [9, 10]. The so-called temperature-glide during evaporation and condensation enables matching the temperature profiles of the heat source and cooling medium, reducing exergy losses [9, 11]. However, mixtures commonly require larger heat transfer areas and, thus, higher capital investment because the heat transfer during evaporation and condensation is reduced due to heat and mass transfer resistances across the vapor and liquid phases [10]. Thus, a thermodynamically beneficial mixture does not guarantee an economic benefit compared to pure components as discussed, e.g., in Refs. [12, 13]. To select optimal mixtures, a rigorous assessment on process level is required, which compares the economic performance of the mixtures capturing all thermo-economic trade-offs.

Due to the challenging trade-off between advantages and disadvantages of mixtures, the identification and use of optimal working fluid mixtures are intensively investigated [11, 14]. However, the identification of optimal mixtures is challenging because the number of possible working fluid mixtures is enormous due to the vast molecular space [15] and the combinatorial complexity. In addition to the mixture components, the mixture composition has to be considered as a continuous degree of freedom. Today, mixture components are commonly selected among well-known pure components based on experience and heuristic guidelines [11]. Subsequently, the preselected working fluid mixtures are assessed in thermo-economic process optimizations. This selection procedure for

mixtures is fast and simple, but suffers from two main shortcomings: First, the preselection is usually limited to a small set of molecules compared to the vast number of molecules which could be considered as components in a mixture. Second, the selection of the working fluid mixture and process optimization are separated despite their strong dependencies. Therefore, a separated approach leads to suboptimal solutions if the preselection of mixture components fails and the actual optimal mixture is excluded [16]. Thus, systematic design methods are required to obtain an optimal combination of working fluid mixture and ORC process. Systematic design methods have to satisfy the following requirements:

1. To capture the vast number of possible molecules and the combinatorial complexity, a computer-aided mixture and blend design (CAM^bD) formulation is required [16].
2. To capture the strong relation between mixtures and processes, the mixtures have to be assessed on the process level by integrating CAM^bD into process design [8, 16, 17].
3. To compute accurate phase behavior of mixtures, a thermodynamic model with strong prediction power for mixtures is needed [18].
4. To capture the impact of mixtures on the economics of the process, detailed sizing of the equipment has to be considered [19].

However, requirement #2, the integration of CAM^bD into process design, leads to a challenging mixed-integer nonlinear programming (MINLP) problem [20]. To tackle the MINLP challenge, several methods for integrated design were developed using CAM^bD as reviewed by Papadopoulos et al. [16]. Integrated design methods have been intensively investigated for pure components using computer-aided molecule design (CAMD), e.g., for the integrated design of pure working fluids [21–29], refrigerants [30, 31] or solvents [32–39]. In contrast, integrated design methods have been less investigated for the design of mixtures.

Several methods have been developed that approximate the integrated design of mixtures and processes by employing heuristic process indicators such

as solubility of a component in the mixture. E.g., Austin et al. [40] proposed a decomposition CAM^bD method and exemplified the method for the design of a solvent/anti-solvent mixture for purification of ibuprofen via cooling crystallization. First, individual bounds are identified for pure component properties, e.g., for solubility parameters. Subsequently, CAM^bD is used to design molecular structures within these bounds and the mixture composition is optimized. Group contribution (GC) methods are used for property prediction. The authors extended the method by property predictions using quantum mechanics calculations [41]. Jonuzaj et al. [42] presented a CAM^bD method based on generalized disjunctive programming (GDP) for the simultaneous identification of the optimal number of mixture components, type of mixture components, and mixture composition. The components of the mixture are chosen from a predefined list of pure candidates. Recently, the authors extended their work to design also the mixture components [43]. The method has been exemplified for the design of solvent/anti-solvent mixtures for crystallization of ibuprofen and for the design of solvent mixtures for separation of acetic acid from water. The methods show the advantages of CAM^bD for the design of mixtures. However, the design employs only process-indicators as assessment criteria and no detailed process model is considered to capture all process-related trade-offs.

To assess the mixtures on the process level, detailed process models have been considered for mixture selection. Molina-Thierry and Flores-Tlacuahuac [44] presented a method to select working fluid mixtures for ORCs. A mixture is initially defined constituting of a set of preselected pure candidates and the mixture composition is optimized to identify the optimal number of components and the type of components. Lee and Mitsos [45] presented a hybrid two-stage method for selecting working fluid mixtures for ORCs. First, the components of the mixture are selected from a list of candidates using stochastic optimization. Subsequently, the composition and process settings are optimized using deterministic optimization. The authors exemplified the method for the recovery of cryogenic energy during evaporation of liquefied natural gas. In these methods,

detailed process models are considered within mixture selection. However, the methods are limited to a predefined list of pure components.

To avoid the limitation to a predefined list of pure components, methods have been developed combining CAM^bD with detailed process models. Buxton et al. [46] developed a decomposition-based method for physical gas absorption. First, candidate mixtures are generated using CAM^bD with property and environmental constraints as well as specific thermodynamic performance tests to reduce the search space. Subsequently, each candidate mixture is individually assessed on the process level using detailed thermo-economic process models. A decomposition-based method has also been proposed by Karunanithi et al. [47] for the design of optimal solvent/anti-solvent mixtures for crystallization of ibuprofen. The search space is first reduced by identifying a set of candidate mixtures based on CAM^bD, which satisfy initially defined constraints on structure, pure component properties, mixture properties, and miscibility. Subsequently, the MINLP problem is solved for the reduced search space considering the process model or, otherwise, individual process optimizations are performed if the number of remaining feasible solutions is small. However, decomposition-based methods can result in suboptimal solutions, if the heuristic property constraints used in the initial procedure to reduce the search space do not capture all trade-offs between process and mixture.

To capture all trade-offs between process and mixture, CAM^bD has been directly combined with detailed process models: Papadopoulos et al. [48] presented an integrated two-stage approach to design binary mixtures for ORCs using a cubic equation of state as thermodynamic model. In the first stage, multi-objective optimization is used to simultaneously optimize the ORC process and the mixture considering chemical feasibility constraints, which are applied for the first component but relaxed for the second component. The optimization results in an optimal first component and a hypothetical, optimal second component. Thus, in a second stage, an optimal second component and composition are identified for the fixed first component. The identified optimal mixtures are assessed and compared to mixtures from literature by Mavrou et al. [49] showing

a better performance of the designed mixtures. Cignitti et al. [50] proposed a hierarchical procedure for the integrated design of processes and binary mixtures using a standard cubic EoS. In their work, the simultaneous optimization on the process level considers both property constraints (e.g., limitations on molecular mass or critical temperature) and process constraints. The authors exemplified their method for a refrigeration process using a local MINLP solver.

The methods show the advantages of an integrated design of processes and mixtures, but thermodynamic property models are used with limited accuracy for mixtures with non-ideal behavior [18]. Furthermore, only thermodynamic process models are considered limiting the approaches to thermodynamic objectives (e.g., thermal efficiency). However, to capture all process-related trade-offs between ORC processes and working fluid mixtures, a thermo-economic assessment criterion is required.

In this work, we present a method for the integrated thermo-economic design of ORC processes and mixtures using an advanced thermodynamic model. The presented method for the design of mixtures is based on our previously presented 1-stage Continuous-Molecular Targeting-Computer-aided Molecular Design (1-stage CoMT-CAMD) method for the integrated design of pure components [24]. In 1-stage CoMT-CAMD, a CAMD formulation is directly linked to a detailed process model to solve the resulting MINLP optimization problem in a single stage. The physically-based perturbed-chain statistically associating fluid theory (PC-SAFT) equation of state [51] is used to model thermodynamic properties. To consider a thermo-economic objective, Schilling et al. [25] directly integrated models for transport properties based on PC-SAFT [52, 53] and detailed models for equipment sizing into 1-stage CoMT-CAMD. The method can be applied for the thermodynamic design of steady state [24] as well as transient applications with off-design operation [54]. Recently, White et al. [28] presented a similar CAMD method for the integrated design of Organic Rankine Cycles using SAFT γ -Mie as the thermodynamic model. The method is illustrated for the design of pure components, but they show the suitability of a SAFT-based

thermodynamic model to predict mixture properties within an integrated design method.

The 1-stage CoMT-CAMD method is extended in this work to the integrated design of ORC processes and binary mixtures, resulting in the 1-stage CoMT-CAM^bD method. The presented method satisfies the requirements needed to identify an optimal combination of mixture and process: A CAM^bD formulation captures an enormous number of possible mixtures within a single MINLP optimization problem. The CAM^bD formulation is directly linked to detailed process models to capture all process-related trade-offs. PC-SAFT provides a consistent thermodynamic model with strong prediction power for mixtures [51] to model both equilibrium and transport properties. Our integrated design method enables not only the thermodynamic design but also the thermo-economic design by integrating detailed models for equipment sizing based on the transport properties of the mixture. With these features, 1-stage CoMT-CAM^bD allows us to identify an optimal combination of ORC processes, equipment, and mixtures based on a thermo-economic objective.

The paper is structured as follows: In section 2, the 1-stage CoMT-CAM^bD method is introduced. 1-stage CoMT-CAM^bD is applied for the integrated design of an Organic Rankine Cycle for waste heat recovery and its working fluid mixture in section 3. In section 4, we discuss the potential of optimal mixtures for Organic Rankine Cycles and show the influence of the mixture composition, the cooling medium and the heat source at the optimum. Finally, conclusions are given in section 5.

2. Framework of 1-stage CoMT-CAM^bD

The presented 1-stage CoMT-CAM^bD method aims at optimizing the thermo-economic performance offered by the molecular design space of binary mixtures used as working fluid for ORCs. Following our work on pure working fluids [25], the thermo-economic design of mixtures can be decomposed into 6 levels (cf. Figure 1): 1 target level, 3 design levels, and 2 connector levels. The target level

defines the economic assessment criterion, usually capturing both capital investment and operating cost (level 1). The calculation of capital investment and operating costs requires the equipment sizes and process settings. The equipment is designed using detailed models for equipment sizing for mixtures (level 2 - design). The sizing models need models for transport properties of mixtures, such as thermal conductivity, as input (level 3 - connector). The process settings are calculated from the design of the process (level 4 - design). The process design needs a model of the process, which in turn requires a thermodynamic model for equilibrium properties of the mixture to calculate all process states (level 5 - connector). In this work, for both connector levels, the physically-based PC-SAFT equation of state is used to model transport as well as equilibrium properties of the mixture in a thermodynamically consistent way. To enable the integrated design of the mixture as a degree of freedom, a computer-aided mixture and blend design (CAM^bD) formulation is used (level 6 - design). Due to the interaction of all levels, an integrated design of processes, equipment, and mixtures is performed in a single optimization problem to capture all inherent thermo-economic trade-offs.

2.1. Problem formulation of 1-stage CoMT-CAM^bD

The MINLP problem for the integrated design of processes, equipment, and mixtures is formulated based on the generic formulation introduced by Gani [20].

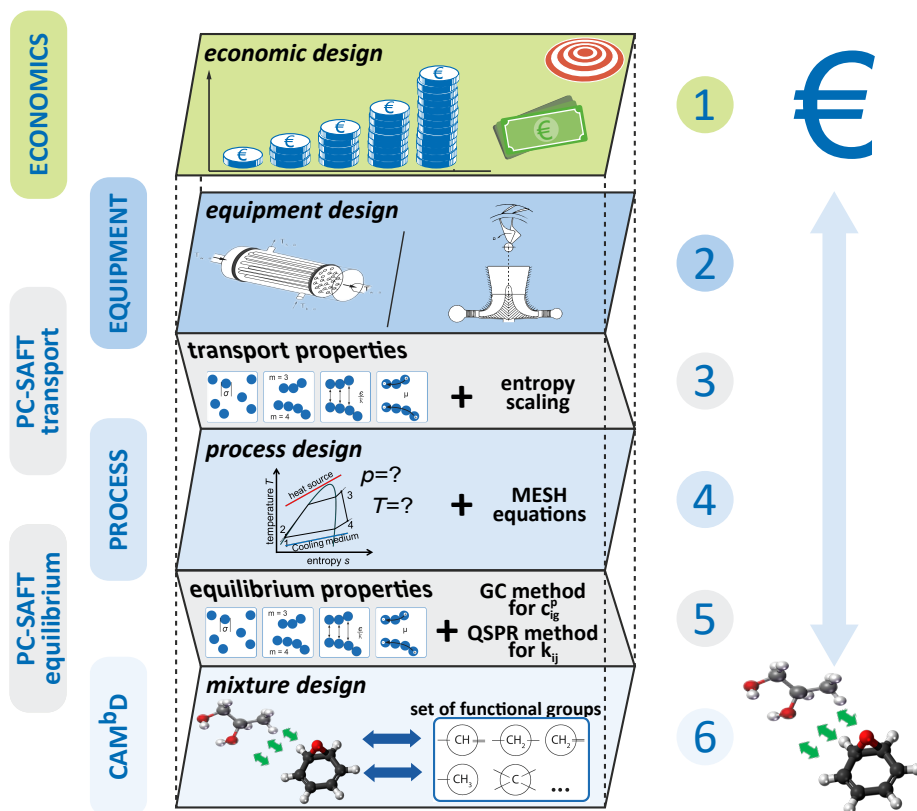


Figure 1: Schematic illustration of the presented 1-stage CoMT-CAM^bD method for integrated thermo-economic design of processes, equipment and mixtures. (adapted from Ref. [25] for the integrated design of mixtures)

In this work, the integrated design of a binary mixture is considered leading to Problem (1):

$$\begin{aligned}
& \min_{x, \xi, y_1^S, y_2^S} f(x, \theta, \kappa) \\
\text{s.t.} \quad & \left. \begin{aligned} g_1(x, \theta, \kappa) &= 0 \\ g_2(x, \theta, \kappa) &\leq 0 \end{aligned} \right\} \text{equipment sizing} \\
& \left. \begin{aligned} \kappa &= k(x, \theta, \xi, y_1^S, y_2^S) \end{aligned} \right\} \text{PC-SAFT (transport)} \\
& \left. \begin{aligned} p_1(x, \theta) &= 0 \\ p_2(x, \theta) &\leq 0 \end{aligned} \right\} \text{process} \\
& \left. \begin{aligned} \theta &= t(x, \xi, y_1^S, y_2^S) \end{aligned} \right\} \text{PC-SAFT (equilibrium)} \quad (1) \\
& \left. \begin{aligned} F_1 \cdot y_i^S &= d & \forall i \in \{1, 2\} \\ F_2 \cdot y_i^S &\leq d & \forall i \in \{1, 2\} \\ c(y_1^S, y_2^S) &\leq 0 \end{aligned} \right\} \text{CAM}^{\text{bD}} \\
& x_{\text{lb}} \leq x \leq x_{\text{ub}} \in \mathbb{R}^n \\
& 0 \leq \xi \leq 1 \in \mathbb{R} \\
& y_{\text{lb}}^S \leq y_i^S \leq y_{\text{ub}}^S \in \mathbb{Z}^1 \quad \forall i \in \{1, 2\}.
\end{aligned}$$

In Problem (1), a thermo-economic objective function f is optimized depending on process and equipment variables x (e.g., mass flow rates), equilibrium properties θ (e.g., densities) and transport properties κ (e.g., thermal conductivities) (level 1 in Figure 1). The process and equipment models include equality constraints g_1, p_1 and inequality constraints g_2, p_2 (levels 2 and 4 - for details, see section 2.2). Both equilibrium properties θ and transport properties κ (levels 3 and 5) are calculated from the molecular structure of the binary mixture components (y_1^S, y_2^S) and the mixture composition ξ using the group-contribution method of PC-SAFT [51, 55] (see section 2.3). The mixture design is integrated into the process design using a CAM^{bD} formulation (level 6). In this CAM^{bD} formulation, each component i is characterized by its molecular structure y_i^S .

The structural feasibility of each molecular structure y_i^S is ensured by equality and inequality constraints (F_1, F_2) [56, 57], which guarantee proper connectivity during optimization. For example, the octet rule ensures no open bond in the molecular structure or individual equations ensure a proper number of functional groups for ring structures or double bonds (for details, see Refs. [56, 57]). Additional CAM^bD constraints c are used to break the symmetry of the molecular design space and to prevent the identification of identical molecular structures of both components.

The degrees of freedom of the MINLP given in Problem (1) are: the continuous variables of the process and equipment x , the composition of the mixture ξ and the discrete molecular structure y_i^S of each component i . The MINLP in Problem (1) is solved to perform the integrated thermo-economic design of processes, equipment, and mixtures. The result of the MINLP is the optimal molecular structure of each component i jointly with the corresponding optimal process, equipment sizes, and composition of the mixture. In general, also non-conventional properties of the mixture, e.g., thermal stability, flammability, environmental impacts or toxicity, have to be assessed to ensure a safe and environmentally friendly application. These non-conventional properties can be considered directly in 1-stage CoMT-CAM^bD if accurate group-contribution methods or quantitative structure-property relationship (QSPR) methods are available [25]. Otherwise, a ranking of mixture candidates can be calculated and then be assessed a posteriori for further criteria. To calculate a ranking of mixture candidates, so-called integer-cut constraints [58] can be used (cf. Figure 2). For this purpose, the MINLP is solved repeatedly while integer-cut constraints exclude previously identified solutions from the molecular design space.

Here, we solve the MINLP using the software GAMS (version 25.1.3 [59]). Stable computation is ensured by performing the computationally demanding iterative calculations of the process, equipment sizing, and PC-SAFT in external functions [25]. We use the local deterministic MINLP solver DICOPT [60], which links an outer-approximation formulation [61] to a relaxation strategy. DICOPT solves a series of NLP subproblems and MILP master problems until

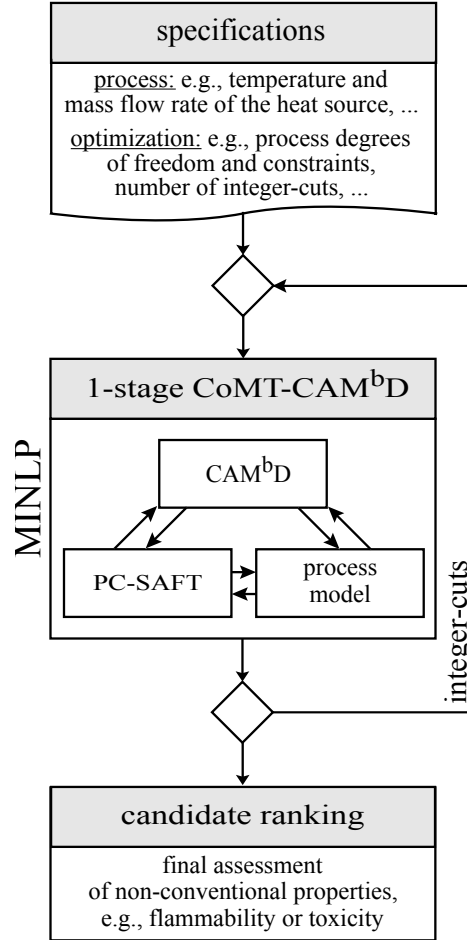


Figure 2: Framework of the presented 1-stage CoMT-CAM^{bD} method. Integer-cuts can be used to obtain a ranked list of optimal mixtures. (adapted from Ref. [24] for the integrated design of mixtures)

a stopping criterion is fulfilled. Initially, a relaxation problem is solved where the integer variables are considered as continuous variables. The relaxed problem yields an optimal, hypothetical mixture, which is called target. The target value is a lower bound of the objective function: no actual mixture will be able to perform better. The potential of the CoMT framework to optimize the target not only of a pure component but also of a mixture has been demonstrated by Lampe et al. [62, 63]. Their work only addressed thermodynamic efficiency and no economics. Most importantly, the PC-SAFT pure component parameters of a binary mixture were relaxed in an integrated design problem. The result was thus an optimal set of PC-SAFT parameters but no actual components. In contrast, the present work directly identifies real mixtures for optimal thermo-economic performance. For this purpose, the problem has been extended by transport properties as well as equipment sizing and costing and by a CAMD formulation. The discrete choices in the design of the equipment and the molecules transform the problem from an NLP to a challenging MINLP. An outer-approximation formulation is used afterwards by the MINLP solver to identify an optimal integer solution. In this work, SNOPT [64] is used as NLP subsolver and CPLEX [65] is used as MILP subsolver.

2.2. Process and equipment models

The models of the process and equipment depend on continuous process and equipment variables x , equilibrium properties θ , and transport properties κ of the mixture. In general, also structural degrees of freedom of the process flowsheet can be considered, e.g., reheating or regeneration [66]. However, in this work, we consider only continuous process variables. Process models enable calculating the operating cost, while equipment models enable calculating the capital investment. Thus, any economic objective function based on operating cost and capital investment can be considered (e.g., net present value). However, also any thermodynamic objective function can be used (e.g., net power output), which would require no sizing of the equipment and model for transport properties. The process and equipment models encompass equality process con-

straints p_1 (e.g., mass and energy balances) and equipment constraints g_1 (e.g., heat transfer correlations) as well as inequality process constraints p_2 (e.g., limits of the minimal approach temperature in the heat exchangers) and equipment constraints g_2 (e.g., limitations of the turbine).

Compared to pure working fluids, mixtures change the fluid behavior within the process by showing a continuous nonlinear temperature change in the 2-phase region due to the change of the vapor/liquid composition during evaporation and condensation. The temperature change affects the pinch analysis and the sizing of the heat exchangers. Since standard pinch constraints assume linear temperature profiles, a more detailed analysis is required to accurately determine the pinch point during evaporation and condensation. Thus, the temperature change during evaporation and condensation is resolved in detail within the process model to capture the impact on the process performance. For this purpose, the temperature in the 2-phase region is discretized in equal intervals and individual vapor/liquid equilibrium calculations are performed to determine the corresponding equilibrium properties, e.g., vapor quality or vapor/liquid enthalpy. The discretization of the temperature shows a more stable and efficient computation compared to a discretization of the vapor quality. The resulting actual temperature change depending on the vapor quality is used for pinch analysis and heat exchanger sizing. Furthermore, mixtures show a reduced overall heat transfer for evaporation and condensation compared to pure components because of heat and mass transfer resistances across the vapor and liquid phases. The reduction of the heat transfer during evaporation and condensation of mixtures is considered by individual correction factors for the heat transfer correlations (for details see Section 3.2).

2.3. CAM^bD based on group-contribution PC-SAFT

To calculate equilibrium and transport properties of the mixture, we use the thermodynamically consistent perturbed-chain statistical associating fluid theory (PC-SAFT) equation of state (EoS) [51] including polar contributions [67, 68]. In PC-SAFT, a molecule is characterized by a set of typically 3 to 7

physically-based pure component parameters z . To calculate mixture properties, the pure component parameters z_i of each component and an additional binary interaction parameter $k_{i,j}$ are required to correct the segment-segment interactions of unlike chains [51]. In this work, no associating and no quadrupolar molecules are considered. Thus, a molecule is described by only 4 pure component parameters: Two pure component parameters characterize the geometry of the molecule which is modeled by a chain: the segment number m captures the length and the segment diameter σ its width. The segment dispersion energy ϵ/k describes the van der Waals attraction and the dipole moment μ describes the dipole interaction. The physical background of the model ensures that these pure component parameters are strongly related to the actual molecular structure, which renders PC-SAFT suitable for optimization based on relaxation strategies.

We link PC-SAFT to the CAM^bD formulation using the homosegmented group contribution method of PC-SAFT [55]. In this GC method, the pure component parameters z_i of each component are calculated from its molecular structure y_i^S representing the component in the CAM^bD formulation. The molecular structure of component i is represented by a vector $y_i^S = (n_{1,i}, n_{2,i}, \dots, n_{l,i})^T$, which contains the number of functional groups $n_{k,i}$ of type k . The pure component parameters z_i are calculated from the molecular structure y_i^S based on mixing rules [69]:

$$\begin{aligned}
z_{i,1} &:= m_i &= \sum_{k \in K} n_{k,i} \cdot m_k, \\
z_{i,2} &:= (m \cdot \sigma^3)_i &= \sum_{k \in K} n_{k,i} \cdot m_k \cdot \sigma_k^3, \\
z_{i,3} &:= (m \cdot \epsilon/k)_i &= \sum_{k \in K} n_{k,i} \cdot m_k \cdot (\epsilon/k)_k, \\
z_{i,4} &:= \mu_i &= \sum_{k \in K} n_{k,i} \cdot \mu_k.
\end{aligned} \tag{2}$$

The group contribution parameters of group k are indicated by $\hat{z}_k = (m_k, \sigma_k, (\epsilon/k)_k, \mu_k)^T$. These parameters have been adjusted to measurement data for vapor-liquid equilibria (VLE) and liquid densities of a database [55].

The pure component parameters of component 1 and component 2 are used to calculate the binary interaction parameter $k_{i,j}$ (here: $k_{1,2}$) based on the QSPR method of Stavrou et al. [70]. Furthermore, the pure component parameters of PC-SAFT are used to break the symmetry of the molecular design space in the inequality constraints c of Problem (1). The best results are obtained for the constraint:

$$(m \cdot \epsilon/k)_1 \leq (m \cdot \epsilon/k)_2, \quad (3)$$

which can be an indication that component 1 is the more volatile component of the mixture.

We use the PC-SAFT equation of state to calculate both equilibrium and transport properties of the mixture. PC-SAFT is based on the residual Helmholtz energy. To calculate absolute properties θ , a reference property is thus required. Here, we use the heat capacity of the ideal gas c_p^{ig} as reference property, which we calculate from the molecular structure y_i^S of component i using the first-order group-contribution method of Joback and Reid [71]. Using the PC-SAFT and the heat capacity of the ideal gas, absolute caloric properties, such as absolute enthalpy differences h of a mixture of 2 components with a mole fraction ξ_i and pure component parameters z_i , can be calculated for a given pressure p and temperature T as sum of a residual (res) and an ideal (id) contribution:

$$\begin{aligned} h(p, T, \xi, y_1^S, y_2^S) &= h^{\text{res}}(p, T, \xi, z_1(y_1^S), z_2(y_2^S)) + h^{\text{id}}(T, \xi, y_1^S, y_2^S) \\ &= \underbrace{h^{\text{res}}(p, T, \xi, z_1(y_1^S), z_2(y_2^S))}_{\text{PC-SAFT}} + \sum_{i=1}^2 \xi_i \cdot \underbrace{\int_{T_0}^T c_p^{\text{ig}}(\tilde{T}, y_i^S) d\tilde{T}}_{\text{Joback}}. \end{aligned} \quad (4)$$

Here, T_0 denotes an arbitrary reference temperature. The phase stability of the mixture is assessed based on the Helmholtz energy as calculated from PC-SAFT. Phase stability is not necessary for the success of an ORC process, but

the considered correlations assume a single phase, e.g., for heat transfer. Thus, no constraint on phase stability is added, but a warning is issued within the integrated design. However, for the final results of the case studies considered in this work, no warning on phase stability is issued (section 3).

The model for transport properties of the mixture κ from PC-SAFT has been proposed by Lötgering-Lin and Gross [72] for viscosities η and by Hopp and Gross [73] for thermal conductivities λ . The models for transport properties are based on Rosenfeld's entropy-scaling [74, 75]. Rosenfeld found that transport properties show a univariate dependence on the residual entropy s^{res} . In the PC-SAFT-based model, transport properties $\kappa = (\eta, \lambda)^{\text{T}}$ are calculated as product of a reduced property $\kappa^* = (\eta^*, \lambda^*)^{\text{T}}$ and a reference property $\kappa^{\text{ref}} = (\eta^{\text{ref}}, \lambda^{\text{ref}})^{\text{T}}$:

$$\kappa = \kappa^* \cdot \kappa^{\text{ref}}. \quad (5)$$

The reduced viscosity η^* and thermal conductivity λ^* of a mixture with n components and mole fractions ξ_i are calculated based on the transport property model for pure components [52, 76]:

$$\ln(\eta^*) = A_\eta + B_\eta s^* + C_\eta s^{*2} + D_\eta s^{*3} \quad (6)$$

$$\ln(\lambda^*) = A_\lambda + B_\lambda s^* + C_\lambda(1 - \exp(s^*)) + D_\lambda s^{*2} \quad (7)$$

using mixing rules for the coefficients $A_\kappa = (A_\eta, A_\lambda)^{\text{T}}$ to $D_\kappa = (D_\eta, D_\lambda)^{\text{T}}$:

$$\begin{aligned} A_\kappa &= (A_\eta, A_\lambda)^{\text{T}} = \sum_{i=1}^n \frac{\xi_i m_i}{\bar{m}} A_{\kappa,i} \\ B_\kappa &= (B_\eta, B_\lambda)^{\text{T}} = \sum_{i=1}^n \frac{\xi_i m_i}{\bar{m}} B_{\kappa,i} \\ C_\kappa &= (C_\eta, C_\lambda)^{\text{T}} = \sum_{i=1}^n \frac{\xi_i m_i}{\bar{m}} C_{\kappa,i} \\ D_\kappa &= (D_\eta, D_\lambda)^{\text{T}} = \sum_{i=1}^n \frac{\xi_i m_i}{\bar{m}} D_{\kappa,i} \end{aligned} \quad (8)$$

and the dimensionless residual entropy of the mixture:

$$s^* = \frac{s^{\text{res}}}{N_A k_B \bar{m}}. \quad (9)$$

Here, $\bar{m} = \sum_{i=1}^n \xi_i m_i$ indicates the average segment number of the mixture and $A_{\kappa,i} = (A_{\eta,i}, A_{\lambda,i})^T$ to $D_{\kappa,i} = (D_{\eta,i}, D_{\lambda,i})^T$ denote the adjustable parameters of the pure component viscosity [52] as well as thermal conductivity [76]. N_A is the Avogadro constant and k_B the Boltzmann's constant. Although the mixing rules for the coefficients of the reduced transport properties ($A_{\kappa,i}$ to $D_{\kappa,i}$) are linear with mole fractions, the resulting transport property is non-linear due to the non-linear contribution of the residual entropy. In previous work, it was seen that viscosities of a binary mixture can for example be lower than the viscosities of both pure substances at given temperature and pressure, in agreement to experimental data [72].

The reference transport properties $\kappa^{\text{ref}} = (\eta^{\text{ref}}, \lambda^{\text{ref}})^T$ of mixtures with n components and mole fractions ξ_i are calculated based on the pure component reference properties according to Wilke [77]:

$$\kappa^{\text{ref}} = \sum_{i=1}^n \frac{\xi_i \cdot \kappa_{\text{pure},i}^{\text{ref}}}{\sum_{j=1}^n \xi_j \cdot \Phi_{ij}} \quad (10)$$

with

$$\Phi_{ij} = \frac{\left(1 + \left(\frac{\kappa_{\text{pure},i}^{\text{ref}}}{\kappa_{\text{pure},j}^{\text{ref}}} \right)^{0.5} \cdot \left(\frac{M_j}{M_i} \right)^{0.25} \right)^2}{\left(8 \cdot \left(1 + \frac{M_i}{M_j} \right) \right)^{0.5}}. \quad (11)$$

Here, $\kappa_{\text{pure},i}^{\text{ref}}$ denotes the pure component reference property of component i for viscosities [52] or thermal conductivities [53]. With these approaches, the viscosity and thermal conductivity of the mixture are predicted accurately from the molecular structure of each component and the mixture composition using PC-SAFT. Lötgering-Lin and Gross determined an average error of less than 7 % for predicted mixture viscosities considering a set of over 120 binary mixtures of n-alkanes, aromatics and cycloalkanes [72]. In this work, we use a pre-

Table 1: Functional groups employed in this work based on Sauer et al. [55].

Molecular family	Groups
(branched) alkanes	$-\text{CH}_3$, $-\text{CH}_2-$, $\text{>CH}-$, >C<
(branched) alkenes	$=\text{CH}_2$, $=\text{CH}-$, >C=
1-alkynes ^a	$-\text{C}\equiv\text{CH}$
aromatics ^b	$\text{>C}^{\text{Arom}}=$, $\text{<CH}^{\text{Arom}}=$
cyclohexanes ^b	$\text{>CH}^{\text{Hex}}-$, $\text{<CH}_2^{\text{Hex}}-$
cyclopentanes ^b	$\text{>CH}^{\text{Pent}}-$, $\text{<CH}_2^{\text{Pent}}-$
aldehydes	$-\text{CH}=\text{O}$
ketones	$\text{>C}=\text{O}$
formates ^a	$-\text{O}-\text{CH}=\text{O}$
ethers	$-\text{O}-\text{CH}_3$, $-\text{O}-\text{CH}_2-$
esters	$-\text{O}-(\text{C}=\text{O})-$

^a only available for thermodynamic design due to limited data available for transport properties.

^b with alkyl side groups

liminary group-contribution method for the thermal conductivity of mixtures, which is based on the model for viscosities. For mixture thermal conductivities, we expect a similar average error as for viscosities. The full extension of the entropy-scaling approach for thermal conductivities to mixtures as well as for diffusion coefficients [78] is currently in progress.

In this work, we use GC methods for the pure component parameters z_i , the heat capacity of the ideal gas $c_{p,i}^{\text{ig}}$, the scaling factors for transport properties $A_{\kappa,i}$ to $D_{\kappa,i}$, and the molar mass M_i . The functional groups employed in this work are limited by the available measurement data. The extrapolation from molecular families contained in the considered measurement data is prevented by additional constraints in the CAM^bD formulation (F_1, F_2) of Problem (1). We employ all functional groups provided by the original works of the GC methods as given in Table 1. Unfortunately, halogenated components are not available yet. The molecular design space of 1-stage CoMT-CAM^bD can be easily extended by additional functional groups as soon as the group-contribution parameters are adjusted to measurement data.

3. Integrated design of Organic Rankine Cycles

We exemplify 1-stage CoMT-CAM^bD for the integrated design of a sub-critical Organic Rankine Cycle without regeneration. The general operating principle of an Organic Rankine Cycle comprises 4 steps (Figure 3): In step 1, the pressure level of the working fluid is increased in the pump to the upper pressure level p_{evap} ($1 \rightarrow 2$). The working fluid is then preheated, evaporated and optionally superheated using the heat source ($2 \rightarrow 3$). In step 3, the turbine expands the working fluid to the lower pressure level p_{cond} ($3 \rightarrow 4$). A generator is used to transform the mechanical work of the turbine into electrical power. Finally, in step 4, the working fluid is condensed and cooled to the initial state in the condenser ($4 \rightarrow 1$).

3.1. General specifications

In this work, we consider a non-regenerated Organic Rankine Cycle based on Chys et al. [79]. Liquid wastewater is used as heat source with an inlet temperature of $T_{\text{HS}}^{\text{in}} = 150^\circ\text{C}$ and a mass flow rate of $\dot{m}_{\text{HS}} = 15 \text{ kg s}^{-1}$ (Table 2). In the condenser, the working fluid mixture is cooled using cooling water with an inlet and outlet temperature of $T_{\text{CW}}^{\text{in}} = 25^\circ\text{C}$ and $T_{\text{CW}}^{\text{out}} = 35^\circ\text{C}$, respectively.

The integrated design of the ORC process is exemplified for a thermodynamic objective as well as for a thermo-economic objective. As thermodynamic objective, we consider the net power output P_{net} calculated as:

$$\begin{aligned} f(x, \theta) = P_{\text{net}}(x, \theta) &= \eta_{\text{G}} \cdot (P_{\text{T}} - P_{\text{P}}) \\ &= \eta_{\text{G}} \cdot \dot{m}_{\text{wf}} \cdot ((h_3 - h_4) - (h_2 - h_1)), \end{aligned} \quad (12)$$

where η_{G} denotes the efficiency of the generator, P_{T} indicates the power output of the turbine and P_{P} denotes the power input of the pump. The total mass flow rate of the working fluid mixture is represented by \dot{m}_{wf} and the enthalpy of the mixture in state i by h_i (cf. Figure 3). The net power output P_{net} is typically used as thermodynamic objective for waste-heat applications because the goal is to exploit the free heat source as much as possible [11].

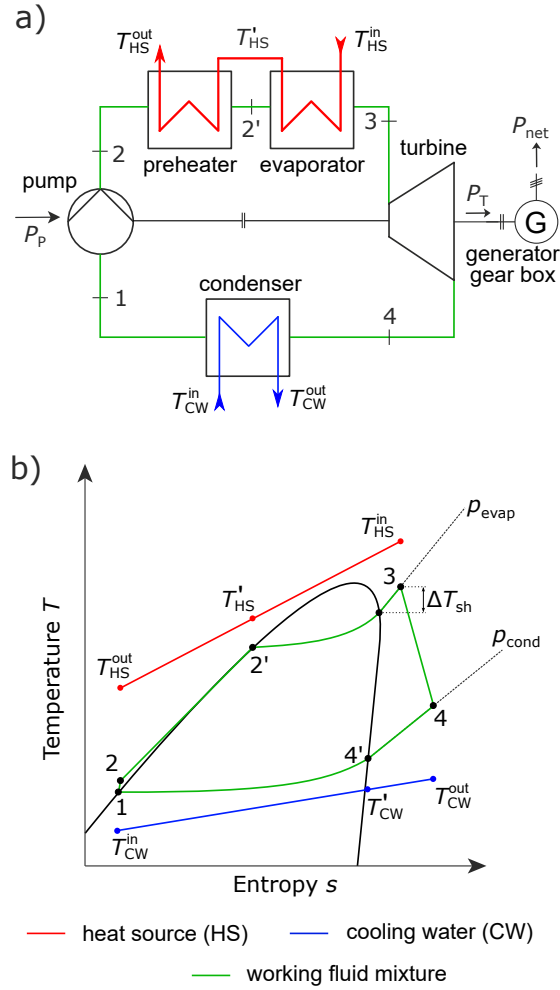


Figure 3: Organic Rankine Cycle using a working fluid mixture in (a) a flowsheet and (b) a temperature-entropy diagram. For illustrative purposes, the temperature levels of the heat source and cooling water are shown in the temperature-entropy diagram at the corresponding states of the working fluid. (adapted from Ref. [25])

As thermo-economic objective, we use the specific investment cost SIC, which is calculated as:

$$f(x, \theta, \kappa) = \text{SIC}(x, \theta, \kappa) = \frac{\text{TCI}(x, \theta, \kappa)}{P_{\text{net}}(x, \theta)} \quad (13)$$

where TCI indicates the total capital investment (for details, see section 3.2). The specific investment cost SIC is commonly used as economic objective of ORCs since fewer assumptions for cost parameters are necessary than, e.g., for the net present value. Such assumptions for cost parameters are often time and location dependent as, e.g., the rate of interest [80].

For both objectives, the process degrees of freedom $x = (\dot{m}_{\text{wf}}, p_{\text{cond}}^{\text{red}}, p_{\text{evap}}^{\text{red}}, \Delta T_{\text{sh}})^{\text{T}}$ are: the total mass flow rate of the working fluid mixture \dot{m}_{wf} , the reduced pressure levels in the condenser $p_{\text{cond}}^{\text{red}}$ as well as the evaporator $p_{\text{evap}}^{\text{red}}$ and the degree of superheating after evaporation ΔT_{sh} . The reduced pressure levels are calculated as $p^{\text{red}} = p/p_{\text{crit}}$ with the absolute pressure level p and the critical pressure of the mixture p_{crit} as calculated from PC-SAFT. We use reduced pressure levels to ensure subcritical processes and a more stable computation by simple bound constraints. The degrees of freedom of the mixture are the molecular structure of each component y_i^{S} and the molar composition ξ .

The pressure drops in heat exchangers are neglected. We consider constant isentropic efficiencies for the pump $\eta_{\text{P, is}} = 0.8$ and the turbine $\eta_{\text{T, is}} = 0.65$ (Table 2). However, in general, the efficiencies can also be calculated based on a detailed turbine or pump model [81, 82]. Condensation at the turbine outlet is constrained to prevent droplet erosion by limiting the vapor quality at the turbine outlet to $\varphi_{\text{min}} = 1$. Furthermore, subcooling after condensation is not considered. The pressure levels are constrained by minimal and maximal absolute pressure levels $(p_{\text{min}}, p_{\text{max}})$ as well as reduced pressure levels $(p_{\text{min}}^{\text{red}}, p_{\text{max}}^{\text{red}})$.

To ensure feasible heat transfer, we limit the minimal approach temperature: For the thermodynamic design, the minimal approach temperature is set to $\Delta T_{\text{E, min}} = 20 \text{ K}$ in the evaporator and to $\Delta T_{\text{C, min}} = 10 \text{ K}$ in the condenser as suggested by Chys et al. [79]. For the thermo-economic design, the optimal

Table 2: General specifications of the ORC case study based on Chys et al. [79].

Parameter	Symbol	Value
Mass flow rate (heat source)	\dot{m}_{HS}	15 kg s^{-1}
Inlet temperature (heat source)	$T_{\text{HS}}^{\text{in}}$	$150 \text{ }^{\circ}\text{C}$
Specific isobaric heat capacity (heat source)	$c_{\text{p,HS}}$	$4,293 \text{ J kg}^{-1} \text{ K}^{-1}$
Inlet temperature (cooling water)	$T_{\text{CW}}^{\text{in}}$	$25 \text{ }^{\circ}\text{C}$
Temperature rise (cooling water)	ΔT_{CW}	10 K
Specific isobaric heat capacity (cooling water)	$c_{\text{p,CW}}$	$4,179 \text{ J kg}^{-1} \text{ K}^{-1}$
Minimal vapor quality (turbine outlet)	φ_{min}	1
Isentropic turbine efficiency	$\eta_{\text{T,is}}$	0.65
Isentropic pump efficiency	$\eta_{\text{P,is}}$	0.8
Generator efficiency	η_{G}	0.97
Minimal absolute pressure	p_{min}	1 bar
Minimal reduced pressure	$p_{\text{min}}^{\text{red}}$	10^{-3}
Maximal absolute pressure	p_{max}	50 bar
Maximal reduced pressure	$p_{\text{max}}^{\text{red}}$	0.8
Maximal segment number	n_{max}	25

minimal approach temperature does not need to be specified, rather it is determined implicitly by the trade-off between net power output and total capital investment. Thus, we just impose a positive minimal approach temperature to obey the second law of thermodynamics. To capture the full temperature profile of the mixture in the 2-phase region, the phase change is discretized into 50 intervals of equal temperature differences (see section 2.2).

Finally, we limit the number of functional groups per molecular structure to $\sum_{k \in K} n_{i,k} \leq n_{\text{max}} = 25$ corresponding to 9,202 structurally feasible pure components for the thermodynamic design and 8,208 for the thermo-economic design. These structurally feasible pure components lead to more than 42 and 33 million structurally feasible mixtures, respectively. The limitation of the number of functional groups per molecular structure stabilizes the optimization. Since the optimal molecules contain much fewer groups, this limit has no impact on the results.

3.2. Sizing and investment models

We calculate the total capital investment TCI from the purchased-equipment cost PEC, which are multiplied by factors for additional direct and indirect

costs [83, 84] (for details see Schilling et al. [25]). The purchased-equipment costs are calculated analogously to Schilling et al. [25] considering the chemical plant cost index (CEPCI) with $\text{CEPCI}_{2017} = 567.5$ [85] to account for inflation and development of raw material prices. For the rotating equipment, the purchased-equipment cost is calculated based on Astolfi et al. [86]. The cost correlation has originally been developed for pure components and turbines with higher power output. Thus, inaccuracies should be expected, but we show the general applicability of a turbine design correlation within our integrated design method. Two turbine design constraints are considered to avoid high Mach numbers and large blade heights in the turbine as recommended by Astolfi et al. [86]. In this work, the number of turbine stages is fixed to $n_{\text{st}} = 1$ since no higher stage number has occurred in previous test cases. For the heat exchangers, the purchased-equipment cost is calculated from the heat exchanger area A_{HE} [87]. In general, the cost correlations are expected to introduce the largest inaccuracies to the model. For a preliminary design as performed in this work, the accuracy range of the cost estimation is expected to range from -20% to 30% [88, 89]. Noteworthy, if the goal is working fluid mixture selection, the variance of the model uncertainties is the main concern to our approach. In contrast, any bias in the model predictions is less relevant as long as the bias affects all mixtures in the same way since the ranking will then not change. Thus, the ranking is usually more robust than the absolute values, since absolute values are affected by both bias and variance of the uncertainties. Still, accurate thermodynamic, process, as well as economic models are the prerequisite to obtain accurate results and differences in performances among the best mixtures have to be considered carefully.

The heat exchangers are modeled as shell-and-tube heat exchangers in counter-flow without shell baffles, which are sized depending on the heat transfer coefficients as introduced by Schilling et al. [25]. We calculate the inner and outer heat transfer coefficients using heat transfer correlations for single-phase, evaporation and condensation (Table 3). The heat transfer correlations depend on dimensionless parameters (e.g., Reynolds or Nusselt number), which

in turn depend on the transport properties of the mixture. Heat transfer for single-phase, forced convection is assumed for: the heating medium, the cooling medium, and the working fluid mixture in the preheater, the superheating part of the evaporator as well as desuperheating part of the condenser. The heat transfer coefficient is here calculated based on the correlation of Gnielinski [90] with mean relative uncertainties of less than 8% [91]. In contrast to single-phase heat transfer, heat transfer of mixtures is reduced during evaporation and condensation due to resistances of the heat and mass transfer [10]. The reduced heat transfer coefficients of mixtures during evaporation and condensation are commonly calculated using a general correlation for pure fluids with a correction factor [92, 93]. In this work, a general correlation for flow boiling of pure fluids is used for evaporation, wherein a superposition of forced convection and bulk boiling is assumed [94]. For forced convection, we use the correlation of Dittus and Boelter [95] with a correction for mixtures based on Bell and Ghaly [96], which has been originally developed for condensation but can be adapted for evaporation [93]. For bulk boiling, the correlation of Cooper [97] with a correction for mixtures based on Thome and Shakir [98] is used. For this procedure, Shah (2015) determined a mean relative deviation of less than 20% comparing predicted heat transfer coefficients to over 700 experimental data points of varying mixtures [93]. For condensation of mixtures, we calculate the heat transfer coefficient using the correlation of Numrich and Müller [99] for filmwise condensation with a correction for mixtures based on Bell and Ghaly [96]. The correlations used for flow boiling and condensation describe the local heat transfer depending on the vapor quality φ . Therefore, we discretize the temperature profile to calculate individual heat transfer areas with constant mean vapor quality (see section 2.2). Furthermore, the heat transfer for flow boiling is described depending on the heat flux density and thus on the heat exchanger area A_{HE} of the evaporator, which is calculated in the sizing model. Thus, we iteratively calculate the heat exchanger area in external functions using fixed-point iteration [100].

Table 3: Correlations for the heat transfer types in the shell-and-tube heat exchangers of the ORC.

Heat transfer	Phenomenon	Reference
single phase	forced convection	Gnielinski [90]
evaporation	flow boiling as superposition of (1) and (2)	Gungor and Winterton [94]
	(1) forced convection correction for mixtures	Dittus and Boelter [95] Bell and Ghaly [96]
	(2) bulk boiling correction for mixtures	Cooper [97] Thome and Shakir [98], Shah [93]
condensation	filmwise condensation	Numrich and Müller [99]
	correction for mixtures	Bell and Ghaly [96]

3.3. Results of 1-stage CoMT-CAM^bD

1-stage CoMT-CAM^bD is used to identify the optimal mixture, the corresponding optimal process and equipment of the case study presented in section 3.1. We exemplify the integrated design of the Organic Rankine Cycle and the working fluid mixture for two objectives: First, the net power output P_{net} is maximized as a thermodynamic objective (section 3.3.1) and second, the specific investment cost SIC is minimized as a thermo-economic objective (section 3.3.2).

The optimization problem consists of 4 continuous process degrees of freedom x , the continuous mole fraction ξ and 100 binary degrees of freedom to characterize the molecular structures of the binary mixture. For the thermo-economic optimization, only 96 binary degrees of freedom are considered, since 2 functional groups are not available due to limited experimental data. The number of binary degrees of freedom of the molecular structure is determined from the considered set of functional groups and the constituting structure constraints, e.g., the maximal number of functional groups. The binary notation of the molecular structure is used for easy implementation of integer-cut constraints [58].

3.3.1. Thermodynamic design

First, the integrated design is performed limiting the outlet temperature of the heat source to $T_{\text{HS}}^{\text{out}} = 135\text{ }^{\circ}\text{C}$ as specified by Chys et al. [79]. The outlet temperature has to be constrained if the remaining heat of the heat source is required in a subsequent process step, e.g., for heat integration.

Initially, 1-stage CoMT-CAM^bD solves the relaxed problem leading to a hypothetical, optimal mixture, the target, with a target value of $P_{\text{net}} = 111\text{ kW}$. The target value serves as an upper bound on the net power output (section 2.1). A ranking of 10 *real* working fluid mixtures is calculated using integer-cuts (Table 4). The resulting ranking consists of mixtures composed of a polar C3 component (ketone, aldehyde, or ester) and a second polar C4-C6 component (ketone, aldehyde, ester, or formate). The mole fraction of the more volatile component is in the range of 45 % to 82 %. For all identified mixtures, the optimal degree of superheating is low (0 K to 5 K). If a higher degree of superheating is required for control reasons, the lower bound of the degree of superheating can be increased within the integrated design.

The best mixture consists of 70 % acetone and 30 % 3-pentanone with a net power output of $P_{\text{net}} = 108\text{ kW}$, which is 2.5 % lower than the target value. While acetone has been discussed as working fluid for ORCs in literature [101], to the best of the authors' knowledge, 3-pentanone as well as the mixture of acetone and 3-pentanone are novel working fluids for ORC applications. Compared to the optimal mixture discussed in Chys et al. [79] (isopentane/hexane with $P_{\text{net}} = 96.2\text{ kW}$), the net power output of acetone/3-pentanone is predicted to be 12 % higher.

In a second scenario, the outlet temperature of the heat source $T_{\text{HS}}^{\text{out}}$ is no more limited but allowed to vary to optimally recover heat from the heat source. The initial relaxed problem leads to a target value of $P_{\text{net}} = 318\text{ kW}$. Thus, the target value is almost 3 times higher compared to the scenario with limited outlet temperature of the heat source, since the heat input is increased. A ranking of 10 *real* working fluid mixtures is calculated using integer-cuts (Table 5). The

Table 4: Target mixture and top 10 mixtures with the corresponding net power output P_{net} and mole fraction of component 1 ξ_1 identified using 1-stage CoMT-CAM^bD. The net power output P_{net} is considered as objective function and the outlet temperature of the heat source is limited to $T_{\text{HS}}^{\text{out}} = 135^\circ\text{C}$.

Rank	Mixture	P_{net} in kW	ξ_1 in %
-	target mixture	110.9	89.4
1	acetone / 3-pentanone ^a	108.1	69.6
2	acetone / 3-methyl-2-butanone	108.1	62.4
3	acetone / 3,3-dimethyl-2-butanone	108.1	81.6
4	propionaldehyde / 2-butanone	107.3	57.7
5	propionaldehyde / pivalaldehyde	107.0	72.6
6	acetone / methyl isobutyrate ^b	107.0	63.6
7	acetone / tert-butyl formate	106.8	55.0
8	methyl acetate / pivalaldehyde	106.2	52.5
9	acetone / pivalaldehyde	106.0	45.8
10	propionaldehyde / methyl propionate ^c	105.3	63.5

^a or isomer 2-pentanone. The first-order GC method does not distinguish among isomers.

^b or isomer isopropyl acetate

^c or isomer ethyl acetate

identified mixtures are composed of propane or propene as the first component and a branched alkane, alkene or ether as second component. Compared to the design with the limited outlet temperature of the heat source, the mole fraction of the more volatile component is on average 31 percentage points higher (83 % to 97 %) leading to optimal mixtures composed of a large amount of the more volatile component. For the identified mixtures, a large amount of the more volatile component is required to optimally match the temperature-glide during condensation and the temperature rise of the cooling water (for details, see Section 4.2.1).

The best mixture consists of 95 % propane and 5 % diethyl ether with a net power output of $P_{\text{net}} = 295\text{ kW}$, which is 7.3 % lower than the target value. Both propane and diethyl ether have been discussed as pure working fluids for ORC applications [11], but to the best of the authors' knowledge, the mixture of propane and diethyl ether is novel. Compared to the optimal mixture discussed in Chys et al. [79] for this case study (isopentane/cyclohexane with $P_{\text{net}} =$

Table 5: Target mixture and top 10 mixtures with the corresponding net power output P_{net} and mole fraction of component 1 ξ_1 identified using 1-stage CoMT-CAM^bD for unlimited outlet temperature of the heat source $T_{\text{HS}}^{\text{out}}$. The net power output P_{net} is considered as objective function.

Rank	Mixture	P_{net} in kW	ξ_1 in %
-	target mixture	318.0	62.0
1	propane / diethyl ether	294.9	94.6
2	propane / 2-methyl-1-butene	294.7	97.0
3	propane / methylbutane	294.1	97.0
4	propene / neopentane	293.7	94.9
5	propene / diethyl ether	293.2	94.2
6	propene / n-butane	293.1	89.5
7	propene / methylbutane	292.5	96.4
8	propene / 2-methyl-1-butene	292.2	96.3
9	propane / neopentane	292.2	95.6
10	propene / isobutane	291.3	83.2

273.8 kW), the net power output of propane/diethyl ether is predicted to be 8 % higher.

Since a local optimization solver is used, the optimal identified mixture can still be a local optimum. Numeric analysis of the results shows that the net power output of propane/diethyl ether is only 0.05 % lower than that of the optimal mixture of an analyzed validation set of 10,585 mixtures (for details see Appendix A). Thus, the mixture identified as optimal does not represent the global optimum but a very good near-optimal solution with a relative difference to the global optimum lower than the expected model uncertainties.

In general, the net power output P_{net} can be increased by reducing exergy losses of the process [102]. Exergy losses during heat input are minimized by adapting the temperature profile of the working fluid mixture to the temperature profile of the heat source. For the design with a limited outlet temperature of the heat source, the heat source temperature is rather flat. Thus, the temperature profile of the heat source can be well followed by mixtures with a wide two-phase region and a high critical temperature (see Figure 4 (top) for acetone/3-pentanone). In contrast, for the design with unlimited outlet temperature of the heat source, the temperature profile is steeper. Thus, the exergy losses

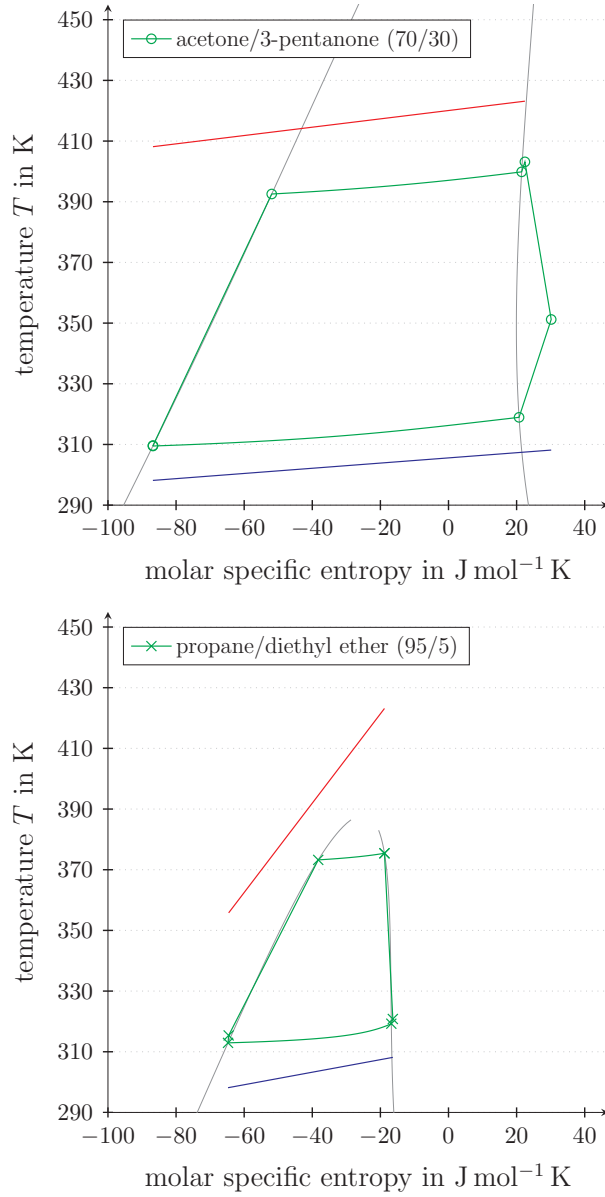


Figure 4: Temperature-entropy diagram of the ORC process for the optimal mixture with limited outlet temperature of the heat source (top: acetone/3-pentanone) and unlimited outlet temperature of the heat source (bottom: propane/diethyl ether) considering the net power output P_{net} as objective. For illustrative purposes, the temperature levels of the heat source (red) and cooling water (blue) are shown at the corresponding states of the working fluid.

are reduced by adapting the temperature profiles during preheating leading to optimal mixtures with a smaller two-phase region and lower critical temperature (see Figure 4 (bottom) for propane/diethyl ether).

3.3.2. Thermo-economic design

Again, the integrated design of the ORC process and mixture is first performed limiting the outlet temperature of the heat source to $T_{\text{HS}}^{\text{out}} = 135^\circ\text{C}$ but now the specific investment cost SIC (Equation (13)) is used as objective. The initial relaxed problem leads to a target value of $\text{SIC} = 6,331\text{ €/kW}$ and a mole fraction of $\xi_1 = 1$. Thus, the lower bound of the objective function is represented by a hypothetical pure working fluid. The 1-stage CoMT-CAM^bD method is not limited to the design of mixtures but can also design pure components, which simply correspond to mole fractions of $\xi_1 = 0$ or $\xi_1 = 1$. A ranking of 10 *real* working fluid mixtures is calculated using integer-cuts (Table 6). In contrast to the target, the optimal real working fluid is not a pure component but a mixture. The identified ranking consists of mixtures composed of propene and a second, less volatile component. The mole fraction of propene is in the range of 70 % to 96 %. The best mixture consists of 94 % propene and 6 % benzene with specific investment cost of $\text{SIC} = 6,980\text{ €/kW}$, which is 10 % higher than the target value. Both propene and benzene are well-known pure working fluids for ORCs [11], but to the best of the authors' knowledge, the mixture has not been discussed for ORCs.

Since previous methods for the integrated design of mixtures and processes only consider thermodynamic objectives, we compare the thermo-economic design to the thermodynamic design as benchmark approach from the literature. Compared to the thermodynamic design with limited outlet temperature of the heat source (Table 4), the identified mixtures have a significantly lower critical temperature and a smaller two-phase region. Furthermore, for all mixtures, a higher degree of superheating of 10 K to 23 K is identified as optimal. The economically optimal mixture propene/benzene leads to a 3 % lower net power output in a thermodynamic process optimization ($P_{\text{net}} =$

Table 6: Target mixture and top 10 mixtures with the corresponding specific investment cost SIC and mole fraction of component 1 ξ_1 identified using 1-stage CoMT-CAM^bD. The specific investment cost SIC is considered as objective function and the outlet temperature of the heat source is limited to $T_{\text{HS}}^{\text{out}} = 135^\circ\text{C}$.

Rank	Mixture	SIC in €/kW	ξ_1 in %
-	target mixture	6,331	100
1	propene / benzene	6,980	94.1
2	propene / methyl acetate	6,982	87.1
3	propene / cyclopentane	6,994	90.2
4	propene / acetone	7,004	87.4
5	propene / methyl cyclopentane	7,019	93.7
6	propene / cyclohexane	7,027	95.9
7	propene / methyl propionate ^a	7,041	89.9
8	propene / 1-butene	7,046	70.4
9	propene / 2-butanone	7,067	93.9
10	propene / isobutane	7,113	71.3

^a or isomer ethyl acetate

104.8 kW with $\xi_1 = 79.7\%$) compared to the thermodynamically optimal mixture acetone/3-pentanone (Table 4). In contrast, the thermo-economic process optimization for acetone/3-pentanone identifies no mixture but pure acetone as optimal ($\xi_1 = 100\%$), which increases the specific investment cost by 88 % (SIC = 13,091 €/kW) compared to the thermo-economically optimal mixture propene/benzene. The thermodynamic design (Table 4) increases volume flow rates of the mixtures due to lower pressure levels and densities leading to higher purchased-equipment cost for the turbine, which is not economically efficient. Consequently, the thermo-economic design prefers working fluid mixtures with higher pressure levels and densities leading to optimal mixtures with a smaller two-phase region and a lower critical temperature. Thus, the assessment of a thermo-economic objective is important to capture all process-related trade-offs.

In a second scenario, the outlet temperature of the heat source $T_{\text{HS}}^{\text{out}}$ is allowed to vary to optimally recover heat from the heat source. The initial relaxed problem leads to a target value of SIC = 3,344 €/kW and again to a hypothetical pure working fluid with a mole fraction of $\xi_1 = 1$. Thus, the target value is 47 % lower compared to the scenario with limited outlet temperature of the heat

Table 7: Target mixture and top 10 mixtures with the corresponding specific investment cost SIC and mole fraction of component 1 ξ_1 identified using 1-stage CoMT-CAM^bD for unlimited temperature of the heat source $T_{\text{HS}}^{\text{out}}$. The specific investment cost SIC is considered as objective function.

Rank	Mixture	SIC in €/kW	ξ_1 in %
-	target mixture	3,344	100
1	propene / propionaldehyde	3,479	93.9
2	propene / acetone	3,493	95.1
3	propene / cyclopentane	3,496	98.0
4	propene / butyraldehyde	3,497	94.7
5	propene / cyclohexane	3,499	97.7
6	propene / methyl acetate	3,503	94.1
7	propene / isobutyraldehyde	3,503	96.9
8	propene / methyl cyclopentane	3,505	97.8
9	propene / 1-butene	3,508	85.6
10	propene / 2-butene	3,511	89.3

source since the specific investment cost tends to decrease with increasing net power output [103]. A ranking of 10 *real* working fluid mixtures is calculated using integer-cuts (Table 7). Again, the identified ranking consists of mixtures with propene as the first component and a second, less volatile component. The best mixture is composed of 94 % propene and 6 % propionaldehyde with specific investment cost of $\text{SIC} = 3,479 \text{ €/kW}$, which is 4 % higher than the target value. To the best of the authors’ knowledge, propionaldehyde and its mixture with propene have not been discussed as working fluid in the state-of-the-art ORC literature. However, acetaldehyde from the same molecular family of propionaldehyde has been recently identified as a promising working fluid for ORC applications by several screening or design approaches [21, 104, 105]. In this work, acetaldehyde is excluded from the design space since small molecules with less than 3 functional groups usually do not lend themselves for a group contribution parametrization. To evaluate acetaldehyde as mixture component in future work, acetaldehyde could be considered within our framework as an individual group as shown in our previous work [54].

A numeric analysis of the results shows that the specific investment cost SIC of propene/propionaldehyde is only 0.07 % lower than that of the global

optimal mixture of an analyzed validation set of 6,670 mixtures (for details see Appendix A). Thus, the optimal identified mixture represents again not the global optimum but a very good near-optimal solution with a relative difference to the global optimum lower than the expected model uncertainties.

Comparing the thermodynamic design (Table 5) and the thermo-economic design (Table 7) for the case of an unlimited outlet temperature of the heat source shows that no mixture is common to both top 10 rankings. However, in contrast to the design with limited outlet temperature of the heat source, the identified mixtures are similar with a more volatile first component propane or propene and a second, less volatile component. Thermodynamic process optimization for the economically optimal mixture propene/propionaldehyde reduces the net power output by 2.5 % ($P_{\text{net}} = 287.5 \text{ kW}$ with $\xi_1 = 96.3 \%$) compared to the thermodynamically optimal mixture propane/diethyl ether (cf. Table 5). In contrast, the thermo-economic process optimization of propane/diethyl ether increases the specific investment cost by 5 % ($\text{SIC} = 3,645 \text{ €/kW}$ with $\xi_1 = 92.9 \%$) compared to the thermo-economically optimal mixture propene/propionaldehyde. Comparing the thermo-economic design for the limited and unlimited outlet temperature of the heat source shows that 6 mixtures are identified in both rankings. The design with unlimited outlet temperature of the heat source increases the average mole fraction of propene by 7 percentage points (85 % to 98 %) and the average degree of superheating by 11 K (25 K to 32 K).

In summary, while the thermodynamic design leads to optimal mixtures that strongly differ for the design with limited and unlimited outlet temperature of the heat source, the identified mixtures are similar if thermo-economic trade-offs are considered. Furthermore, the design with unlimited outlet temperature of the heat source leads to similar mixtures for both, thermodynamic and thermo-economic optimizations due to the steep temperature of the heat source. The individual, optimal mixtures of the case studies discussed in Section 3.3 are identified from the inherent trade-offs between economics, process and mixture. These trade-offs can usually not be captured by simplified criteria for mixture

selection based on experience and heuristic guidelines. The results thus highlight the need for an integrated thermo-economic design of ORC processes and mixtures.

4. Potential of optimal mixtures for Organic Rankine Cycles

In this section, we compare the potential of optimal working fluid mixtures for Organic Rankine Cycle to optimal pure working fluids (section 4.1). Furthermore, the influence of the mixture composition (section 4.2), the cooling medium (section 4.3) and the heat source temperature (section 4.4) is analyzed. In the following, only the case with unlimited outlet temperature of the heat source is considered, which is the more common case.

4.1. Mixtures vs. pure components

Mixtures are considered as working fluids for Organic Rankine Cycles due to their favorable thermodynamic properties compared to pure components. The continuous change of the temperature during evaporation and condensation enables the match of the temperature profile of the mixture to the temperature profile of the heat source and the cooling medium reducing exergy losses during heat transfer and increasing net power output. In contrast, however, the heat transfer coefficient of mixtures is reduced during evaporation and condensation, leading to larger heat transfer areas and higher capital investment. To quantify these effects, optimal mixtures designed by 1-stage CoMT-CAM^bD are compared to optimal pure components designed by 1-stage CoMT-CAMD [24, 25].

4.1.1. Thermodynamic Design

Maximizing the net power output P_{net} , the optimal pure component is propane with a net power output of $P_{\text{net}} = 276 \text{ kW}$ (Table 8). The net power output of the optimal mixture is 7% higher than the net power output of the optimal pure component confirming the potential of mixtures from a thermodynamic point of view [9, 11]. However, the thermodynamic potential of the mixture is comparatively small since propane is already a good pure working

Table 8: Target and top 5 pure components identified using 1-stage CoMT-CAMD and the corresponding maximized net power output P_{net} .

Rank	Pure component	P_{net} in kW
-	target	280.5
1	propane	276.1
2	propene	264.3
3	isobutane	246.2
4	n-butane	244.0
5	isobutene	242.7

fluid for the given process specifications resulting in a high mole fraction of propane in the optimal mixture (for a comparison to other case studies see section 4.3 and 4.4).

Figure 5 (top) compares the temperature-entropy (T - s) diagram of the optimal mixture propane/diethyl ether (95%/5%) to that of the optimal pure component propane. For both, mixture and pure component, superheating is avoided. For pure propane, the temperature profiles of the heat source and the working fluid show already a good match during preheating limiting exergy losses. The optimal mixture shows a higher critical temperature and a wider 2-phase region. Furthermore, the temperature-glide of the mixture enables a better match of the temperature profiles, in particular for the cooling medium. Consequently, the mixture has a higher net power output despite the reduced cooling of the heat source. The temperature-entropy diagram shows that liquid droplets could occur during expansion since the expansion is not modeled in detail and only the outlet vapor quality of the turbine is constrained. If regarded as critical, this behavior could be avoided by imposing a higher minimal degree of superheating constraining vapor quality during expansion or by a detailed model of the turbine [81].

4.1.2. Thermo-economic Design

Minimizing the specific investment cost SIC, the optimal pure component is propene with specific investment cost of $\text{SIC} = 3,587 \text{ €/kW}$ (Table 9). Thus, the optimal mixture reduces the specific investment cost by 3.0 % compared to

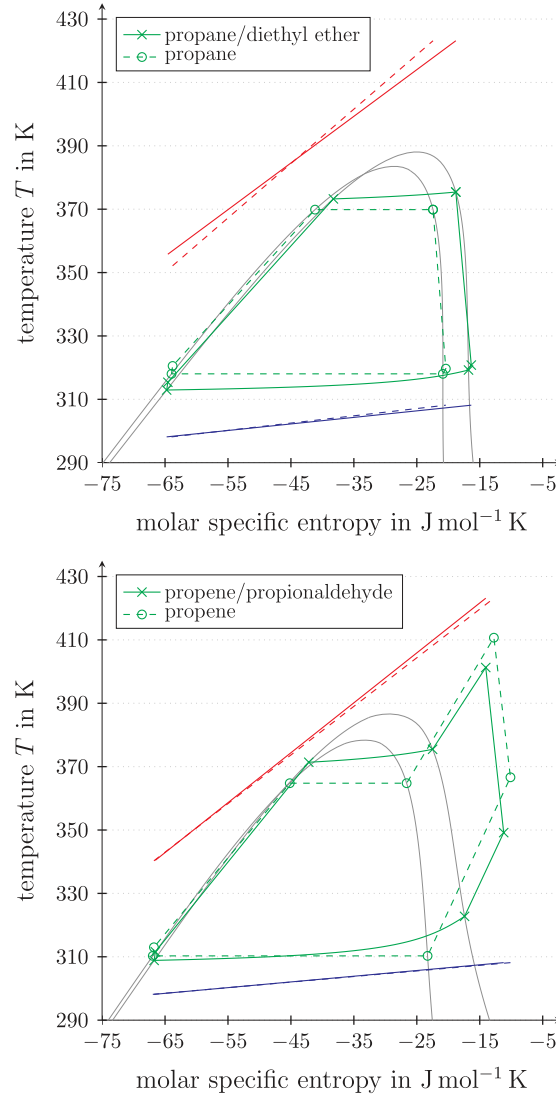


Figure 5: Temperature-entropy diagram of the optimal mixture (solid lines) and pure component (hatched lines) considering the net power output P_{net} (top) and the specific investment cost SIC (bottom) as objective. For illustrative purposes, the temperature levels of the heat source (red) and cooling water (blue) are shown at the corresponding states of the working fluid.

the optimal pure component. The optimal mixture propene/propionaldehyde (94%/6%) requires a 23% (22 m^2) larger heat exchanger area for preheating, mainly caused by smaller temperature differences and larger heat flow, even

Table 9: Target and top 5 pure components identified using 1-stage CoMT-CAMD and the corresponding minimized specific investment cost SIC.

Rank	Pure component	SIC in €/kW
-	target	3,344
1	propene	3,587
2	propane	3,667
3	1-butene	4,559
4	isobutene	4,570
5	isobutane	4,616

though the thermal conductivity of the mixture is 2.6 % larger than for pure propene. The heat exchanger areas for evaporation and condensation are 49 % (16 m²) and 9 % (18 m²) larger, respectively, since the heat flow is larger and the heat transfer is reduced for mixtures during evaporation and condensation. In contrast to evaporation, the relative increase in the heat exchanger area for condensation is much smaller. In the condenser, the temperature differences are larger compared to the pure working fluid propene due to the temperature-glide of the mixture during condensation (see Figure 5 - bottom). The larger temperature differences compensate for the reduced heat transfer in the condenser. For both, mixture and pure component, the vapor is superheated after evaporation. However, the mixture has a smaller degree of superheating compared with the pure working fluid leading to a 52 % (26 m²) and 60 % (40 m²) smaller heat exchanger area for superheating and desuperheating, respectively. The reduced heat exchanger areas additionally result from a larger thermal conductivity of the mixture (4.3 % and 0.5 % larger for superheating and desuperheating, respectively).

In summary, the total heat exchanger area is reduced for the optimal mixture despite the reduced heat transfer for evaporation and condensation. Consequently, the purchased-equipment cost of heat exchangers is reduced by 1.3 %. At the same time, the net power output of the optimal mixture is increased by 4.3 % compared to pure propene leading to 2.4 % higher purchased-equipment cost of the rotating equipment. Overall, the total capital investment is only 1.0 % higher for the mixture resulting in 3.0 % lower specific investment cost.

Thus, working fluid mixtures can reduce the specific investment cost, in particular, if the optimal pure component has a high degree of superheating. However, the thermo-economic potential of mixtures is lower than the thermodynamic potential, which is in line with literature findings [12, 13, 19]. Thus, an integrated analysis and a careful selection of mixtures are necessary to obtain a thermo-economically optimal combination of process and mixture.

4.2. Influence of the mixture composition

The performance of mixtures as working fluid depends strongly on mixture composition. To investigate the influence, we discretize the mixture composition and perform individual process optimizations for each composition. For both thermodynamic and thermo-economic objectives, the influence of composition is investigated for 4 mixtures:

- the optimal mixture identified by 1-stage CoMT-CAM^bD (thermodynamic: propane/diethyl ether, thermo-economic: propene/propionaldehyde);
- isobutane/isopentane and isopentane/isohexane, which are commonly discussed as working fluid mixtures for ORCs [11, 12, 106];
- the target, consisting of two hypothetical, optimal components with pre-defined composition. For every composition, the target is individually optimized.

4.2.1. Thermodynamic Design

Figure 6 (top) shows the optimal net power output depending on the mole fraction of the more volatile component. The dependence on mixture composition is even qualitatively very different for the investigated mixtures: The mixtures can have a single maximum of the net power output, but also two (local) maxima and one minimum. Furthermore, the maxima can be differentiable but also non-differentiable leading to a kink in the objective. This qualitatively different behavior of the mixtures is explained in the following.

The mixtures propane/diethyl ether and isobutane/isopentane have two local maxima and one local minimum of the net power output. The maxima can be explained by the temperatures in the condenser. The maxima at a smaller

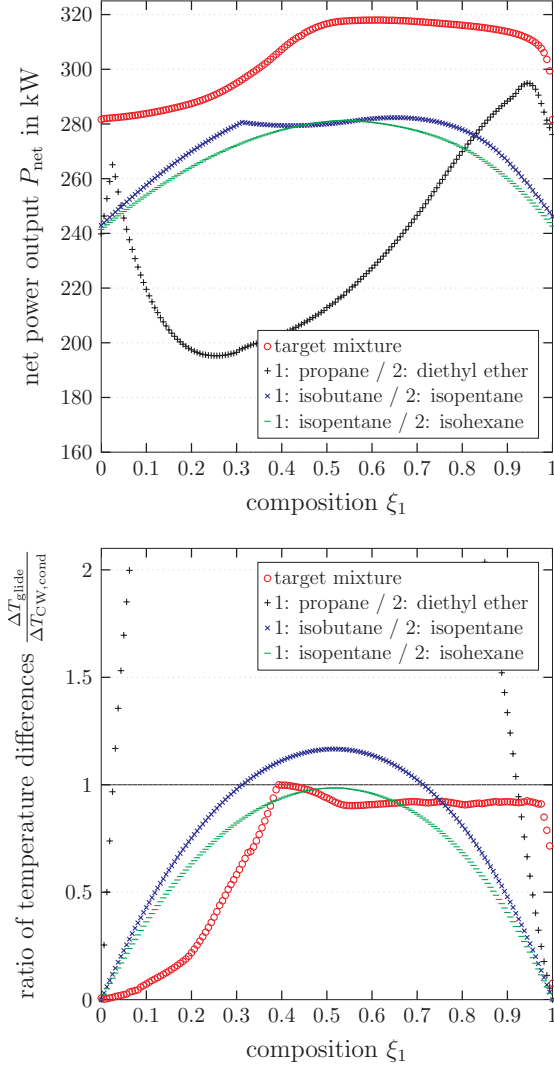


Figure 6: Top: Net power output P_{net} depending on the molar composition for 4 mixtures. The target is individually optimized for each composition and thus it differs along the composition. Bottom: The corresponding ratio of the temperature-glide of the mixture during condensation ΔT_{glide} and the temperature rise of the cooling water $\Delta T_{\text{CW,cond}}$.

mole fraction of the more volatile component occur exactly at the composition for which the temperature-glide during condensation ΔT_{glide} matches the temperature rise of the cooling water $\Delta T_{\text{CW,cond}}$, i.e., $\Delta T_{\text{glide}}/\Delta T_{\text{CW,cond}} = 1$ (Figure 6 - bottom). For higher mole fractions of the more volatile component, the temperature-glide increases and the ratio $\Delta T_{\text{glide}}/\Delta T_{\text{CW,cond}}$ exceeds a value of 1. As a result, the location of the pinch changes from the beginning of condensation (state 4' in Figure 3) to the condenser outlet (state 1) [107]. Thus, for $\Delta T_{\text{glide}}/\Delta T_{\text{CW,cond}} = 1$, a double pinch exists where the pinch criterion is fulfilled simultaneously at the beginning and end of condensation. A double pinch significantly increases efficiency, as shown by Zebian and Mitsos [108].

The match of the temperature-glide to the cooling water is the key to reach the maximum net power output. However, the two maxima show qualitatively different dependence on composition: at low mole fractions of the more volatile component, the maximum is non-differentiable, while the maximum is differentiable at high mole fractions of the more volatile component. The maximum is non-differentiable due to the fact that the pinch position jumps from the beginning to the end of the condensation. Due to the lower mole fraction of the more volatile component, the curvature of the temperature profile during condensation is concave ($\partial^2 T/\partial \varphi^2 < 0$). Consequently, the nonlinear temperature profile is closest to the cooling water temperature at the beginning and end of condensation leading to a sharp change of the pinch from the beginning of condensation to the condenser outlet and thus to a kink in the objective. In contrast, for the maxima at a higher mole fraction of the more volatile component, the curvature of the temperature profile during condensation is partly convex ($\partial^2 T/\partial \varphi^2 > 0$). Here, the location of the pinch changes smoothly from the condenser outlet to the beginning of condensation leading to a smooth maximum, since no double pinch exists. Due to the smooth change of the pinch location, the temperature ratio at the maximum is not exactly 1 since the maximum is not only determined by the temperature-glide but also by the convex curvature of the temperature profile during condensation ($\Delta T_{\text{glide}}/\Delta T_{\text{CW,cond}} = 0.7$ for propane/diethyl ether and $\Delta T_{\text{glide}}/\Delta T_{\text{CW,cond}} = 1.1$ for isobutane/isopentane).

In contrast, the mixture isopentane/isohexane has only one maximum of the net power output. For this mixture, the temperature ratio $\Delta T_{\text{glide}}/\Delta T_{\text{CW,cond}}$ is always lower than 1. Thus, the pinch does not reach the condenser outlet and only one smooth maximum of the net power output is found at almost equimolar composition from the trade-off between temperature-glide and curvature of the temperature profile.

For the mixtures isopentane/isohexane and isobutane/isopentane, the temperature ratio and thus the net power output is rather robust to changes in the composition. In contrast, propane/diethyl ether is more sensitive and a constant composition has to be ensured.

For the target mixture, the pure component with $\xi_1 = 0$ has a net power output of $P_{\text{net}} = 280.5 \text{ kW}$. Due to the constraint to break the symmetry of the design space $((m \cdot \epsilon/k)_1 \leq (m \cdot \epsilon/k)_2)$, component 1 is typically the more volatile component (lower $m \cdot \epsilon/k$). For small mole fractions of the more volatile component (component 1), the net power output increases slowly because also the optimal temperature-glide increases slowly (Figure 6 - bottom). To increase the temperature-glide for these compositions, the pressure-level has to be decreased which would be unfavorable for the thermodynamic performance. For higher mole fractions of the more volatile component 1, the curvature of the temperature profile during condensation is partly convex such that the pinch is located in the 2-phase region. The target identifies an optimal trade-off between temperature-glide and curvature of the temperature profile for a temperature ratio of around $\Delta T_{\text{glide}}/\Delta T_{\text{CW,cond}} = 0.9$. For $\xi_1 = 1$, the pure component with $P_{\text{net}} = 280.5 \text{ kW}$ is identified again.

In summary, various mixtures show qualitatively different dependence on the mixture composition depending on the temperature-glide and the curvature of the temperature profile during condensation. The thermodynamic optimum of the mixture results from an optimal combination of the temperature-glide and the curvature of the temperature profile during condensation. In this case study, the optimum is mostly influenced by the heat transfer in the condenser. However, in general, also the heat transfer in the evaporator can influence the

optimum. Thus, both, the temperature-glide and the curvature of the temperature profile during evaporation and condensation have to be captured within the integrated design, e.g., by discretization of the vapor quality in the heat exchanger models.

4.2.2. Thermo-economic Design

Figure 7 (top) shows the optimal specific investment cost SIC depending on the mole fraction of the more volatile component. The target mixture consists of two components with almost equal molecular structures. Thus, the mixture composition has almost no influence on the specific investment cost and the thermo-economically optimal working fluid is represented by a pure working fluid (see section 3.3.2). For the target, an optimal degree of superheating of 18 K to 21 K is identified (Figure 7 - bottom). Superheating increases the heat exchanger areas for evaporator and condenser. However, the mass flow rate and the sizing parameter of the turbine is reduced, leading to a trade-off between purchased-equipment costs of the rotating equipment and the heat exchangers.

Mixtures can reduce the specific investment cost SIC if the optimal pure component has a high optimal degree of superheating and thus requires large heat exchangers for superheating and desuperheating (see section 4.1.2). The mixtures isobutane/isopentane and isopentane/isohexane achieve minimal specific investment cost SIC for the pure components isobutane and isopentane, respectively. For these pure components, the optimal degree of superheating is 0 K (Figure 7 - bottom). Thus, the mixtures cannot benefit from reducing superheating and the corresponding purchased-equipment cost of the heat exchangers. As a result, the specific investment cost SIC monotonously increase for smaller mole fraction of the less volatile component.

In contrast to pure isobutane and isopentane, pure propene has a comparatively high optimal degree of superheating leading to local minima for the optimal mixture propene/propionaldehyde. For a high mole fraction of propene, the mixture reduces the optimal degree of superheating compared to pure propene

and thus the purchased-equipment cost for the evaporator and condenser (see section 4.1.2). A local minimum is obtained from the trade-off between the reduction of both superheating and heat transfer during evaporation and condensation of mixtures and an increase in turbine size. The specific investment cost SIC increases for lower mole fractions of propene, in particular, as soon as

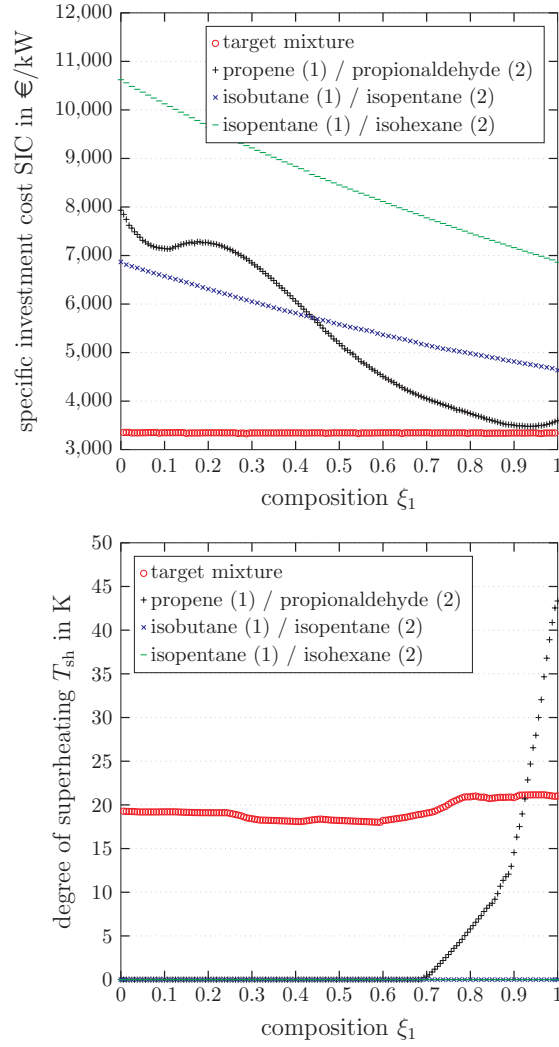


Figure 7: Top: Specific investment cost SIC depending on the molar composition for 4 mixtures. The target is individually optimized for each composition. Bottom: The corresponding optimal degree of superheating T_{sh} .

the degree of superheating reaches $T_{\text{sh}} = 0 \text{ K}$ at $\xi_1 = 0.7$. For a mole fraction of propene of $\xi_1 = 0.1$, the mixture propene/propionaldehyde has a second local minimum of the specific investment cost SIC. Here, a double pinch in the condenser leads to a strong peak of the net power output. The trade-off between net power output and purchased-equipment cost of the rotating equipment results in a local minimum of the specific investment cost.

Overall, mixtures can reduce the specific investment cost SIC, in particular, if the optimal pure component has a high degree of superheating. Otherwise, pure components are preferred and mixtures have no economic benefit. This behavior has to be considered in detail within the integrated design to obtain thermo-economically optimal mixtures.

4.3. Influence of cooling water

The temperature rise of the cooling water has a strong influence on the optimal mixture since the temperature-glide of the mixture during condensation is adapted to match the temperature rise of the cooling water (section 4.2.1). To analyze this effect in more detail, the temperature rise of the cooling water is varied from $\Delta T_{\text{CW}} = 0 \text{ K}$ to 25 K . For each temperature rise, the optimal mixture as well as the optimal pure component are calculated based on a top 10 ranking considering the net power output P_{net} (Figure 8 - top) and the specific investment cost SIC (Figure 8 - bottom) as objective.

For $\Delta T_{\text{CW}} = 0 \text{ K}$, the mixture has no benefit compared to pure components and 1-stage CoMT-CAM^bD identifies propane as the optimal working fluid maximizing the net power output. The specific investment cost SIC cannot be calculated for $\Delta T_{\text{CW}} = 0 \text{ K}$ since sensible heat transfer is assumed for the cooling water in the sizing model, which would lead to an infinite mass flow rate. With increasing temperature rise of the cooling water, the optimal net power output P_{net} decreases sharply for the thermodynamically optimal pure component. Here, the lower pressure level has to be increased to fulfill pinch constraints in the condenser leading to higher exergy losses. Consequently, the optimal specific investment cost SIC also increases sharply for the thermo-

economically optimal pure component due to the trade-off between decreasing net power output and increasing specific investment cost [103]. In contrast, the optimal mixture is able to adapt the temperature-glide during condensation to match the temperature rise of the cooling water leading to a smaller decrease of the net power output P_{net} and a smaller increase of the specific investment cost SIC compared to the optimal pure component. For $\Delta T_{\text{CW}} = 25 \text{ K}$, the

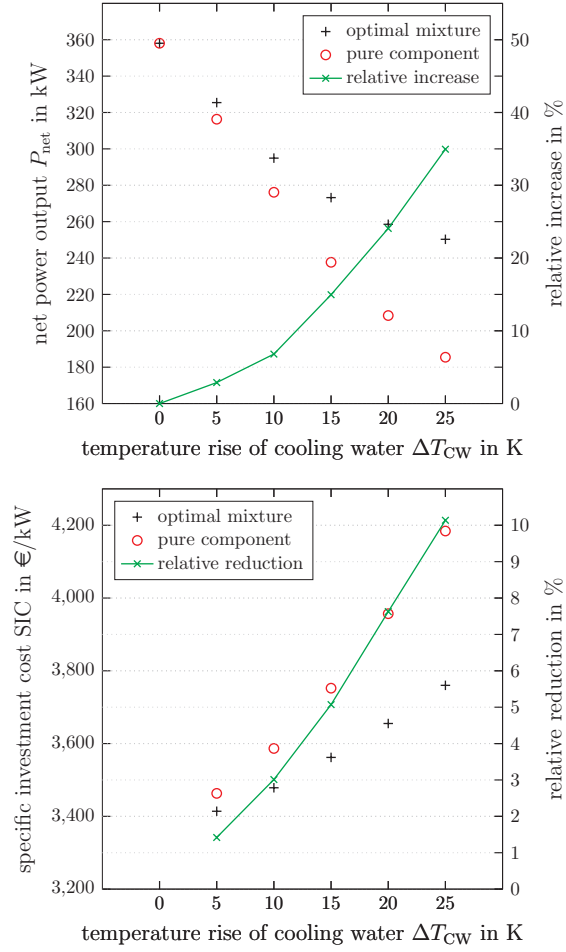


Figure 8: Net power output P_{net} (top) and specific investment cost SIC (bottom) of the optimal mixture and pure component for varying temperature rise of the cooling water ΔT_{CW} . Additionally, the relative increase (top) and reduction (bottom) of the objective is shown, respectively.

optimal mixtures increase the net power output P_{net} by 35 % and reduce the specific investment cost SIC by 10 % compared to the corresponding optimal pure working fluid. Thus, the temperature rise of the cooling medium has a lower impact on the optimal specific investment cost SIC than on the optimal net power output P_{net} . For pure components, not only the net power output but also the capital investment is lower since the purchased-equipment cost of the condenser and rotating equipment is reduced due to larger temperature differences and lower power output, respectively.

The optimal pure components are propane or propene for the thermodynamic objective (P_{net}) depending on the temperature rise of the cooling water, whereas solely propene is identified for the thermo-economic objective (SIC). For the thermodynamic objective, the optimal mixture is composed of propane or propene and a second, less volatile component, which changes from C4 to C5 alkanes with an increasing temperature rise of the cooling water. Furthermore, the mole fraction of the more volatile component decreases to $\xi_1 = 60 \%$ for $\Delta T_{\text{CW}} = 25 \text{ K}$. For the thermo-economic objective, the optimal mixture is propene/propionaldehyde for all cases with decreasing mole fraction of propene from $\xi_1 = 95 \%$ to 89 % with an increasing temperature rise of the cooling water. Thus, the thermodynamically optimal mixture varies for an increasing temperature rise of the cooling medium, while the thermo-economically optimal mixture does not change for this case study. Due to the strong interdependence, the optimal mixture has to be designed systematically for the corresponding process specifications.

4.4. Influence of heat source temperature

To further assess the impact of process specifications, the inlet temperature of the heat source is varied from $T_{\text{HS}}^{\text{in}} = 100^\circ\text{C}$ to 200°C . For each inlet temperature of the heat source, the optimal mixture and pure component are calculated based on a top 10 ranking. The net power output P_{net} (Figure 9 - top) and the specific investment cost SIC (Figure 9 - bottom) are considered as objective.

For the thermodynamic design, the optimal mixtures increase the net power output P_{net} compared to the optimal pure component. The increase ranges from $\Delta P_{\text{net}} = 19 \text{ kW}$ to 100 kW (6 % to 54 %) depending on the inlet temperature of the heat source $T_{\text{HS}}^{\text{in}}$. The net power output increases only slightly by mixtures if the optimal pure component has already a good thermodynamic performance due to a good match of the temperature profiles of the heat source and the

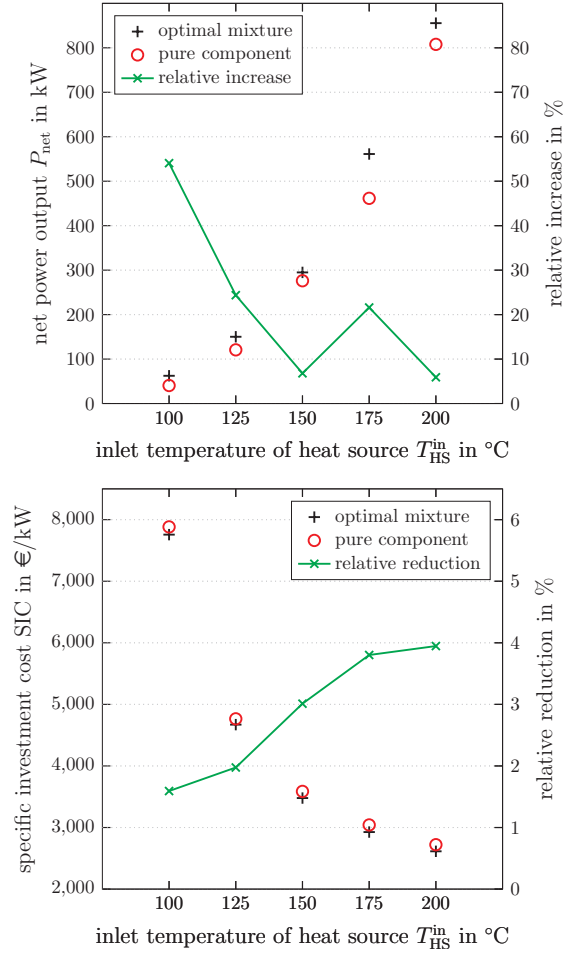


Figure 9: Net power output P_{net} (top) and specific investment cost SIC (bottom) of the optimal mixture and pure component for varying inlet temperature of the heat source $T_{\text{HS}}^{\text{in}}$. Additionally, the relative increase (top) and reduction (bottom) of the objective is shown, respectively.

working fluid during preheating, i.e., for $T_{\text{HS}}^{\text{in}} = 150\text{ }^{\circ}\text{C}$, with an increase in P_{net} of 7 % for the optimal mixture as compared to pure propane (see section 4.1.1) and for $T_{\text{HS}}^{\text{in}} = 200\text{ }^{\circ}\text{C}$, with an increase in P_{net} of only 6 % for the optimal mixture as compared to pure isobutene. In contrast, for $T_{\text{HS}}^{\text{in}} = 175\text{ }^{\circ}\text{C}$, pure C3 components are limited by the maximum pressure leading to higher exergy losses during evaporation. For pure C4 components, in turn, pinch constraints in the preheater limit the adaption of the temperature profiles of the heat source and the working fluid leading to higher exergy losses during preheating. These limitations can be counteracted by using a mixture, which increases the net power output P_{net} by $\Delta P_{\text{net}} = 100\text{ kW}$ (22 %) for $T_{\text{HS}}^{\text{in}} = 175\text{ }^{\circ}\text{C}$ compared to the optimal pure component. The thermodynamically optimal pure components are C3 alkanes for $T_{\text{HS}}^{\text{in}} = 100\text{ }^{\circ}\text{C}$ to $175\text{ }^{\circ}\text{C}$ and a C4 alkane for $T_{\text{HS}}^{\text{in}} = 200\text{ }^{\circ}\text{C}$. In contrast, the optimal mixture varies for all inlet temperatures of the heat source and no simple dependency is found.

For the thermo-economic design, the specific investment cost SIC decreases sharply with an increasing inlet temperature of the heat source due to the increasing net power output. The optimal mixtures decrease the specific investment cost SIC compared to the optimal pure component (1.6 % to 3.9 %). However, the absolute difference between the specific investment cost SIC of the optimal mixture and the optimal pure component is roughly constant ($\Delta\text{SIC} = 94\text{ €/kW}$ to 126 €/kW). Thus, the inlet temperature of the heat source $T_{\text{HS}}^{\text{in}}$ has only a small impact on the economic potential of optimal mixtures. The thermo-economically optimal pure component is propene for all inlet temperatures, while the optimal mixture is composed of propene and a less volatile component, which varies for the different temperatures.

In summary, the heat source inlet temperature has a strong impact on the optimal mixture for a thermodynamic objective, while the impact is comparably small for a thermo-economic objective. Furthermore, the heat source inlet temperature $T_{\text{HS}}^{\text{in}}$ has less impact on the economic potential of mixtures than the temperature rise of the cooling water ΔT_{CW} (see section 4.3). No general rule on the optimal mixture and the potential of mixtures compared to pure

components can be found. Thus, an integrated design of mixtures, processes and equipment is required for the specific process conditions.

5. Conclusions

In this work, we present a method for the integrated thermo-economic design of mixtures, processes and equipment for Organic Rankine Cycles using an advanced thermodynamic model. The method is based on our previously presented 1-stage CoMT-CAMD method, which is extended for the design of binary working fluid mixtures to the so-called 1-stage CoMT-CAM^bD method. A CAM^bD formulation is used to capture a vast number of possible mixtures within a single MINLP optimization. The PC-SAFT equation of state provides a physically-based thermodynamic model to predict both equilibrium and transport properties of mixtures. Detailed models for the process and equipment sizing allow us to assess mixtures on an economic process-level and to capture all process-related trade-offs within the integrated design. In particular, the heat exchangers of the Organic Rankine Cycle are sized using detailed heat transfer correlations for single phase, evaporation and condensation of mixtures. With these features, 1-stage CoMT-CAM^bD enables the holistic design of thermo-economically optimal mixtures and corresponding optimal process settings and equipment sizes.

1-stage CoMT-CAM^bD is successfully exemplified for the integrated design of a subcritical Organic Rankine Cycle, considering a thermodynamic and a thermo-economic objective. Our method efficiently identifies the most promising mixtures, which maximize the net power output or minimize the specific investment cost. The comparison to optimal pure components shows the potential of using working fluid mixtures. In particular, the net power output can be increased by 7% for the presented case study. In contrast, for a thermo-economic objective, the benefit of mixtures is in general lower compared to pure components. However, mixtures can reduce the specific investment cost if the optimal pure component has a high optimal degree of superheating.

We show that both temperature-glide and curvature of the temperature profile during evaporation and condensation, have to be considered in detail during the design to capture all inherent trade-offs. A parameter study of the temperature rise of the cooling medium shows that the potential of mixtures increases with increasing temperature rise. In contrast, for an increasing inlet temperature of the heat source, the economic potential increases, while no clear trend in the thermodynamic benefit can be found. The optimal identified mixture strongly depends on the considered process specifications. Thus, a systematic method is required capturing all process-related trade-offs to design overall optimal mixture and the corresponding optimal process and equipment. Such a systematic design is provided by the presented 1-stage CoMT-CAM^bD method, which is an efficient method for the integrated, thermo-economic design of ORC processes, equipment and mixtures. In future work, the models for equipment sizing and costing have to be validated, since these models are expected to introduce the largest inaccuracies to the model, in particular, for the turbine and heat transfer correlations. Furthermore, a detailed turbine model has to be considered within the integrated design framework to capture the impact of the mixtures on the isentropic efficiency and crucial design parameters of the turbine [81, 82]. Additionally, improved correlations for heat exchanger sizing have to be regarded, which account for pressure drops. To ensure a safe and environmentally friendly application, the identified mixtures have to be assessed regarding non-conventional properties, e.g., flammability, toxicity, thermal stability or environmental impacts.

Acknowledgements

We thank the Deutsche Forschungsgemeinschaft (DFG) for funding this work (BA2884/4-2 and GR 2948/2-2).

Appendix A. Numerical validation of local optimization

In 1-stage CoMT-CAM^bD, a local optimization solver is used since the process and PC-SAFT calculations are performed in external functions to ensure stable computation (see section 2.1). Global optimization methods for implicit functions are only under development [109, 110]. Thus, global optimization of the integrated design problem cannot be applied today. In the following, the quality of the results of Section 3.3 is numerically assessed for the design with an unlimited outlet temperature of the heat source. To assess the efficiency of the presented method, we also analyze the computational effort.

The quality of the optimal solution is assessed by generating a subset of mixtures considered in the CAM^bD formulation and performing a brute-force, individual process optimization of each mixture subsequently. Since the rankings identified by 1-stage CoMT-CAM^bD contain only small molecular structures with $\sum_{k \in K} n_{i,k} \leq 7$, we assume unfavorable thermodynamic behavior of larger molecular structures in this low-temperature case study. Thus, all mixtures are generated with components composed of less than or equal to 7 functional groups. With this limitation, 146 molecular structures are structurally feasible for thermodynamic objectives leading to a subset of 10,585 mixtures. For thermo-economic objectives, 116 molecular structures are structurally feasible, leading to a subset of 6,670 mixtures. In the following, the subsets are called *validation set*. The subsets are comparatively small, but still, the computational effort is tremendous to confirm global optimality using enumerative search. Each mixture of both validation sets is assessed by performing an individual thermodynamic or thermo-economic process optimization. From the individual process optimizations, the *real* ranking for both objectives is obtained. The *real* ranking provides a measure for the quality of the ranking identified by 1-stage CoMT-CAM^bD.

For the thermodynamic design, almost all individual process optimizations of the validation set converge. The best mixture of the validation set is the mixture composed of 98 % propane and 2 % 2-butyl ethyl ether with a net power output

of $P_{\text{net}} = 295.1 \text{ kW}$ (Figure A.10 - top). The best mixture identified with 1-stage CoMT-CAM^{bD} (propane/diethyl ether) shows a 0.05 % lower net power output than the best mixture of the validation set (rank 3 of the validation set). Comparing the net power output of each rank of the identified top 10 ranking and the top 10 ranking of the validation set leads to a maximum deviation of less than 1 %.

For the thermo-economic design, 77 % of the individual process optimizations of the validation set converge, of which in turn 69 % converge to an optimal pure component. The best mixture of the validation set is the mixture composed of 93 % propene and 7 % 1-pentene with specific investment cost of SIC = 3,457 €/kW (Figure A.10 - bottom). The best mixture identified by 1-stage CoMT-CAM^{bD} (propene/propionaldehyde) shows 0.7 % higher specific investment cost than the best mixture of the validation set (rank 3 of the validation set). Comparing the specific investment cost of each rank of the identified top 10 ranking and the top 10 ranking of the validation set leads to a maximum deviation of less than 0.8 %.

Thus, both top 10 rankings identified by 1-stage CoMT-CAM^{bD} show good accordance with the ranked validation sets. The results of 1-stage CoMT-CAM^{bD} are very close to the global optimum of the validation sets and good near-optimal solutions are identified. The relative differences between the objective function values of the optimal mixture of the validation set and the optimal mixture identified by 1-stage CoMT-CAM^{bD} are lower than the expected model uncertainties. Thus, the local MINLP solver performs well, but integer-cut constraints are needed to identify all good solutions. To increase the chance to find the globally optimal solution, the number of integer-cuts can be increased.

To assess the computational effort, the number of function evaluations of the process model are evaluated. The individual process optimizations of the validation sets need 1,787,707 function evaluations for maximizing the net power output and 1,909,706 function evaluations for minimizing the specific investment cost. In contrast, to calculate a ranking of 10 mixtures, 1-stage CoMT-CAM^{bD} requires 3,906 function evaluations for the net power output and 7,369 function

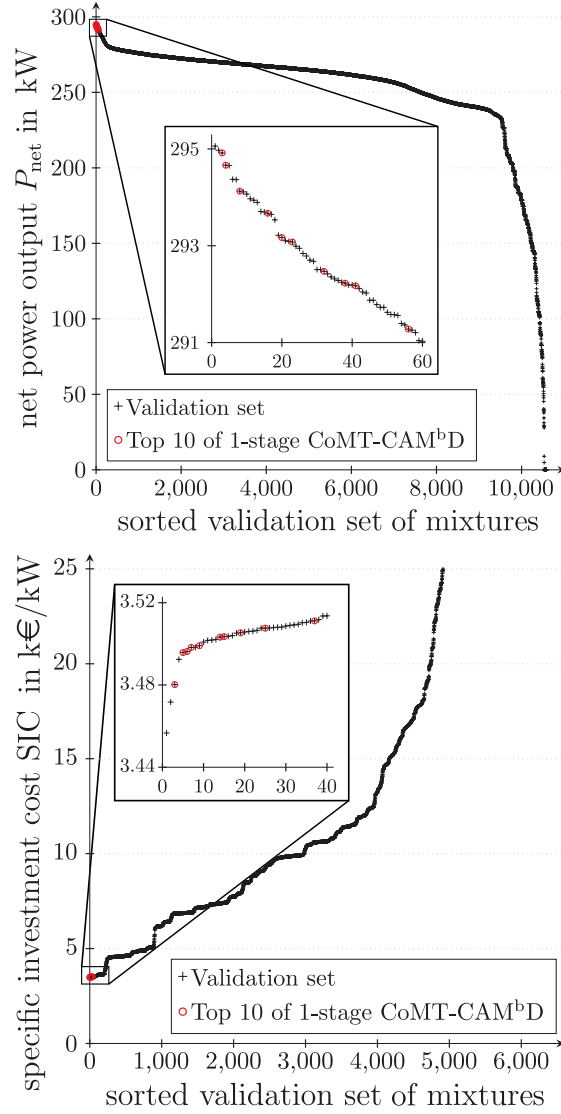


Figure A.10: Optimal net power output P_{net} (top) and optimal specific investment cost SIC (bottom) of all mixtures contained in the validation sets ($\sum_k n_k \leq 7$). Additionally, circles mark the Top 10 mixtures identified using 1-stage CoMT-CAM^{bD}.

evaluations for the specific investment cost (corresponding to 16 min for the net power output and 173 min for the specific investment cost using an Intel-Xeon CPU with 3.0 GHz and 64 GB RAM). Thus, a saving of over 99.5 % in the computational effort can be achieved by using 1-stage CoMT-CAM^bD while considering over 4,000 times more mixtures within the design space. Therefore, 1-stage CoMT-CAM^bD is an efficient method for the integrated design of ORC processes, equipment and mixtures.

References

- [1] Lee I, Tester JW, You F. Systems analysis, design, and optimization of geothermal energy systems for power production and polygeneration: State-of-the-art and future challenges. *Renew Sust Energ Rev* 2019;109:551–77.
- [2] Aboelwafa O, Fateen SEK, Soliman A, Ismail IM. A review on solar Rankine cycles: Working fluids, applications, and cycle modifications. *Renew Sust Energ Rev* 2018;82:868–85.
- [3] Ling-Chin J, Bao H, Ma Z, Taylor W, Paul Roskilly A. State-of-the-art technologies on low-grade heat recovery and utilization in industry. In: Al-Bahadly IH, editor. *Energy conversion: Current Technologies and Future Trends*. London: IntechOpen. ISBN 978-1-78984-904-2; 2019, p. 55–74.
- [4] Xu B, Rathod D, Yebi A, Filipi Z, Onori S, Hoffman M. A comprehensive review of Organic Rankine Cycle waste heat recovery systems in heavy-duty diesel engine applications. *Renew Sust Energ Rev* 2019;107:145–70.
- [5] Mondejar M, Andreasen J, Pierobon L, Larsen U, Thern M, Haglind F. A review of the use of organic Rankine cycle power systems for maritime applications. *Renew Sust Energ Rev* 2018;91:126–51.
- [6] Colonna P, Casati E, Trapp C, Mathijssen T, Larjola J, Turunen-Saaresti T, et al. Organic Rankine Cycle power systems: From the concept to

- current technology, applications, and an outlook to the future. *J Eng Gas Turbines Power* 2015;137(10):100801.
- [7] Tchanche BF, Lambrinos G, Frangoudakis A, Papadakis G. Low-grade heat conversion into power using Organic Rankine Cycles—A review of various applications. *Renew Sust Energ Rev* 2011;15(8):3963–79.
 - [8] Linke P, Papadopoulos A, Seferlis P. Systematic Methods for Working Fluid Selection and the Design, Integration and Control of Organic Rankine Cycles - A Review. *Energies* 2015;8(6):4755–801.
 - [9] Angelino G, Di Paliano PC. Multicomponent working fluids for Organic Rankine Cycles (ORCs). *Energy* 1998;23(6):449–63.
 - [10] Abadi GB, Kim KC. Investigation of Organic Rankine Cycles with zeotropic mixtures as a working fluid: Advantages and issues. *Renew Sust Energ Rev* 2017;73:1000–13.
 - [11] Bao J, Zhao L. A review of working fluid and expander selections for Organic Rankine Cycle. *Renew Sust Energ Rev* 2013;24:325–42.
 - [12] Heberle F, Brüggemann D. Thermo-Economic Evaluation of Organic Rankine Cycles for Geothermal Power Generation Using Zeotropic Mixtures. *Energies* 2015;8(3):2097–124.
 - [13] Oyewunmi OA, Markides CN. Thermo-economic and heat transfer optimization of working-fluid mixtures in a low-temperature Organic Rankine Cycle system. *Energies* 2016;9(6):448.
 - [14] Imran M, Haglind F, Asim M, Alvi JZ. Recent research trends in organic Rankine cycle technology: A bibliometric approach. *Renew Sust Energ Rev* 2018;81:552–62.
 - [15] Fink T, Bruggesser H, Reymond JL. Virtual exploration of the small-molecule chemical universe below 160 Daltons. *Angew Chem Int Ed* 2005;44(10):1504–8.

- [16] Papadopoulos AI, Tsivintzelis I, Linke P, Seferlis P. Computer-Aided Molecular Design: Fundamentals, Methods, and Applications. In: Reedijk J, editor. Reference module in chemistry, molecular sciences and chemical engineering. Elsevier. ISBN 9780124095472; 2018, p. 1–76.
- [17] Adjiman CS, Galindo A, Jackson G. Molecules matter: the expanding envelope of process design. In: Eden MR, editor. Proceedings of the 8th International Conference on Foundations of Computer-Aided Process Design; vol. 34 of Computer-aided chemical engineering. Amsterdam: Elsevier. ISBN 978-0-444-63433-7; 2014, p. 55–64.
- [18] Kontogeorgis GM, Folas GK. Thermodynamic Models for Industrial Applications. Chichester, UK: John Wiley & Sons, Ltd; 2010.
- [19] Andreasen JG, Kærn MR, Haglind F. Assessment of Methods for Performance Comparison of Pure and Zeotropic Working Fluids for Organic Rankine Cycle Power Systems. *Energies* 2019;12(9):1783.
- [20] Gani R. Chemical product design: Challenges and opportunities. *Comput Chem Eng* 2004;28(12):2441–57.
- [21] Papadopoulos AI, Stijepovic M, Linke P. On the systematic design and selection of optimal working fluids for Organic Rankine Cycles. *Appl Therm Eng* 2010;30(6-7):760–9.
- [22] Lampe M, Stavrou M, Bückner HM, Gross J, Bardow A. Simultaneous Optimization of Working Fluid and Process for Organic Rankine Cycles Using PC-SAFT. *Ind Eng Chem Res* 2014;53(21):8821–30.
- [23] Lampe M, Stavrou M, Schilling J, Sauer E, Gross J, Bardow A. Computer-aided molecular design in the continuous-molecular targeting framework using group-contribution PC-SAFT. *Comput Chem Eng* 2015;81:278–87.
- [24] Schilling J, Lampe M, Gross J, Bardow A. 1-stage CoMT-CAMD: An approach for integrated design of ORC process and working fluid using PC-SAFT. *Chem Eng Sci* 2017;159:217–30.

- [25] Schilling J, Tillmanns D, Lampe M, Hopp M, Gross J, Bardow A. From molecules to dollars: Integrating molecular design into thermo-economic process design using consistent thermodynamic modeling. *Mol Syst Des Eng* 2017;2(3):301–20.
- [26] Cignitti S, Andreasen JG, Haglind F, Woodley JM, Abildskov J. Integrated working fluid-thermodynamic cycle design of Organic Rankine Cycle power systems for waste heat recovery. *Appl Energ* 2017;203:442–53.
- [27] White MT, Oyewunmi OA, Haslam AJ, Markides CN. Industrial waste-heat recovery through integrated computer-aided working-fluid and ORC system optimisation using SAFT- γ Mie. *Energ Convers Manage* 2017;150:851–69.
- [28] White MT, Oyewunmi OA, Chatzopoulou MA, Pantaleo AM, Haslam AJ, Markides CN. Computer-aided working-fluid design, thermodynamic optimisation and thermoeconomic assessment of ORC systems for waste-heat recovery. *Energy* 2018;161:1181–98.
- [29] van Kleef LM, Oyewunmi OA, Markides CN. Multi-objective thermo-economic optimization of Organic Rankine Cycle (ORC) power systems in waste-heat recovery applications using computer-aided molecular design techniques. *Applied Energy* 2019;251:112513.
- [30] Roskosch D, Atakan B. Reverse engineering of fluid selection for thermodynamic cycles with cubic equations of state, using a compression heat pump as example. *Energy* 2015;81:202–12.
- [31] Samudra AP, Sahinidis NV. Optimization-based framework for computer-aided molecular design. *AIChE J* 2013;59(10):3686–701.
- [32] Bardow A, Steur K, Gross J. Continuous-Molecular Targeting for Integrated Solvent and Process Design. *Ind Eng Chem Res* 2010;49(6):2834–40.

- [33] Stavrou M, Lampe M, Bardow A, Gross J. Continuous Molecular Targeting–Computer-Aided Molecular Design (CoMT–CAMD) for Simultaneous Process and Solvent Design for CO₂ Capture. *Ind Eng Chem Res* 2014;53(46):18029–41.
- [34] Pereira FE, Keskes E, Galindo A, Jackson G, Adjiman CS. Integrated Design of CO₂ Capture Processes from Natural Gas. In: Kikkinides ES, Pistikopoulos EN, Georgiadis MC, editors. *Energy systems engineering. Process systems engineering*; Weinheim: Wiley-VCH. ISBN 9783527631292; 2008, p. 231–48.
- [35] Pereira FE, Keskes E, Galindo A, Jackson G, Adjiman CS. Integrated solvent and process design using a SAFT-VR thermodynamic description: High-pressure separation of carbon dioxide and methane. *Comput Chem Eng* 2011;35(3):474–91.
- [36] Burger J, Papaioannou V, Gopinath S, Jackson G, Galindo A, Adjiman CS. A hierarchical method to integrated solvent and process design of physical CO₂ absorption using the SAFT- γ Mie approach. *AIChE J* 2015;61(10):3249–69.
- [37] Gopinath S, Jackson G, Galindo A, Adjiman CS. Outer approximation algorithm with physical domain reduction for computer-aided molecular and separation process design. *AIChE J* 2016;62(9):3484–504.
- [38] Scheffczyk J, Fleitmann L, Schwarz A, Lampe M, Bardow A, Leonhard K. COSMO-CAMD: A framework for optimization-based computer-aided molecular design using COSMO-RS. *Chem Eng Sci* 2017;159:84–92.
- [39] Scheffczyk J, Schäfer P, Fleitmann L, Thien J, Redepenning C, Leonhard K, et al. COSMO-CAMPD: a framework for integrated design of molecules and processes based on COSMO-RS. *Mol Sys Des Eng* 2018;3(4):645–57.

- [40] Austin ND, Samudra AP, Sahinidis NV, Trahan DW. Mixture design using derivative-free optimization in the space of individual component properties. *AIChE J* 2016;62(5):1514–30.
- [41] Austin ND, Sahinidis NV, Trahan DW. A COSMO-based approach to computer-aided mixture design. *Chem Eng Sci* 2017;159:93–105.
- [42] Jonuzaj S, Akula PT, Kleniati PM, Adjiman CS. The formulation of optimal mixtures with generalized disjunctive programming: A solvent design case study. *AIChE J* 2016;62(5):1616–33.
- [43] Jonuzaj S, Gupta A, Adjiman CS. The design of optimal mixtures from atom groups using Generalized Disjunctive Programming. *Comp Chem Eng* 2018;116:401–21.
- [44] Molina-Thierry DP, Flores-Tlacuahuac A. Simultaneous Optimal Design of Organic Mixtures and Rankine Cycles for Low-Temperature Energy Recovery. *Ind Eng Chem Res* 2015;54(13):3367–83.
- [45] Lee U, Mitsos A. Optimal multicomponent working fluid of Organic Rankine Cycle for exergy transfer from liquefied natural gas regasification. *Energy* 2017;127:489–501.
- [46] Buxton A, Livingston AG, Pistikopoulos EN. Optimal design of solvent blends for environmental impact minimization. *AIChE J* 1999;45(4):817–43.
- [47] Karunanithi AT, Achenie LE, Gani R. A computer-aided molecular design framework for crystallization solvent design. *Chem Eng Sci* 2006;61(4):1247–60.
- [48] Papadopoulos AI, Stijepovic M, Linke P, Seferlis P, Voutetakis S. Toward Optimum Working Fluid Mixtures for Organic Rankine Cycles using Molecular Design and Sensitivity Analysis. *Ind Eng Chem Res* 2013;52(34):12116–33.

- [49] Mavrou P, Papadopoulos AI, Stijepovic MZ, Seferlis P, Linke P, Voutetakis S. Novel and conventional working fluid mixtures for solar Rankine cycles: Performance assessment and multi-criteria selection. *Appl Therm Eng* 2015;75:384–96.
- [50] Cignitti S, Mansouri SS, Woodley JM, Abildskov J. Systematic optimization-based integrated chemical product–process design framework. *Ind Eng Chem Res* 2018;57(2):677–88.
- [51] Gross J, Sadowski G. Perturbed-Chain SAFT: An Equation of State Based on a Perturbation Theory for Chain Molecules. *Ind Eng Chem Res* 2001;40(4):1244–60.
- [52] Lötgering-Lin O, Gross J. Group Contribution Method for Viscosities Based on Entropy Scaling Using the Perturbed-Chain Polar Statistical Associating Fluid Theory. *Ind Eng Chem Res* 2015;54(32):7942–52.
- [53] Hopp M, Gross J. Thermal Conductivity of Real Substances from Excess Entropy Scaling Using PCP-SAFT. *Ind Eng Chem Res* 2017;56(15):4527–38.
- [54] Schilling J, Eichler K, Kölsch B, Pischinger S, Bardow A. Integrated design of working fluid and Organic Rankine Cycle utilizing transient exhaust gases of heavy-duty vehicles. *Appl Energy* 2019;255:113207.
- [55] Sauer E, Stavrou M, Gross J. Comparison between a Homo- and a Heterosegmented Group Contribution Approach Based on the Perturbed-Chain Polar Statistical Associating Fluid Theory Equation of State. *Ind Eng Chem Res* 2014;53(38):14854–64.
- [56] Struebing H. Identifying optimal solvents for reactions using quantum mechanics and computer-aided molecular design. PhD thesis; Imperial College London; London; 2011.
- [57] Struebing H, Adjiman CS, Galindo A. Optimal solvent design for reactions using computer-aided molecular design. 2011.

URL: <http://www.minlp.org/library/problem/mod/index.php?lib=MINLP&i=180&pi=-137>; (accessed on November 09, 2015).

- [58] Grossmann IE, Kravanja Z. Mixed-integer nonlinear programming techniques for process systems engineering. *Comput Chem Eng* 1995;19:189–204.
- [59] Corporation GD. GAMS – Documentation, GAMS Release 25.1.3. 2018. URL: <https://www.gams.com/latest/docs/gams.pdf>.
- [60] Grossmann IE, Viswanathan J, Vecchietti A, Raman R, Kalvelagen E. GAMS/DICOPT: A discrete continuous optimization package. GAMS Corporation Inc 2002;.
- [61] Duran MA, Grossmann IE. An outer-approximation algorithm for a class of mixed-integer nonlinear programs. *Math Program* 1986;36(3):307–39.
- [62] Lampe M, Edel P, Schilling J, Gross J, Bardow A. Integrated design of working fluid mixtures and Organic Rankine Cycles (ORC) in the Continuous-Molecular Targeting (CoMT) framework. In: V. Lemort, S. Quoilin, M. De Paepe and M. van den Broek , editor. *Proceedings of the 3rd International Seminar on ORC Power Systems ASME-ORC 2015*; vol. 1. 2015, p. 32–40.
- [63] Lampe MHF. Integrated Design of Process and Working Fluids for Organic Rankine Cycles. PhD thesis; RWTH Aachen University; 2016.
- [64] Gill PE, Murray W, Saunders MA. SNOPT: An SQP Algorithm for Large-Scale Constrained Optimization. *SIAM J Optim* 2002;12(4):979–1006.
- [65] IBM Corporation . IBM ILOG CPLEX Optimization Studio, Version 12.6.3. 2016.
- [66] Schilling J, Horend C, Bardow A. Integrating superstructure-based design of molecules, processes, and flowsheets. *AIChE Journal* 2020;66(5):e16903.

- [67] Gross J. An equation-of-state contribution for polar components: Quadrupolar molecules. *AIChE J* 2005;51(9):2556–68.
- [68] Gross J, Vrabec J. An equation-of-state contribution for polar components: Dipolar molecules. *AIChE J* 2006;52(3):1194–204.
- [69] Vijande J, Piñeiro MM, Bessièrès D, Saint-Guirons H, Legido JL. Description of PVT behaviour of hydrofluoroethers using the PC-SAFT EOS. *Phys Chem Chem Phys* 2004;6(4):766–70.
- [70] Stavrou M, Bardow A, Gross J. Estimation of the binary interaction parameter k_{ij} of the PC-SAFT Equation of State based on pure component parameters using a QSPR method. *Fluid Phase Equilib* 2016;416:138–49.
- [71] Joback KG, Reid RC. Estimation of pure-component properties from group-contributions. *Chem Eng Commun* 1987;57(1-6):233–43.
- [72] Lötgering-Lin O, Fischer M, Hopp M, Gross J. Pure Substance and Mixture Viscosities Based on Entropy Scaling and an Analytic Equation of State. *Ind Eng Chem Res* 2018;57(11):4095–114.
- [73] Hopp M, Mele J, Lötgering-Lin O, Gross J. Transport Properties from Entropy Scaling using the PCP-SAFT Equation of State. Boulder, Co, USA: NIST Symposium of Thermophysical Properties; 2018,.
- [74] Rosenfeld Y. Relation between the transport coefficients and the internal entropy of simple systems. *Physical Review A* 1977;15(6):2545–9.
- [75] Rosenfeld Y. A quasi-universal scaling law for atomic transport in simple fluids. *J Phys Condens Matter* 1999;11(28):5415–27.
- [76] Hopp M, Gross J. Thermal conductivity from entropy scaling: A group-contribution method. *Ind Eng Chem Res* 2019;58(44):20441–9.
- [77] Wilke C. A viscosity equation for gas mixtures. *J Chem Phys* 1950;18(4):517–9.

- [78] Hopp M, Mele J, Gross J. Self-Diffusion Coefficients from Entropy Scaling using the PCP-SAFT equation of state. *Ind Eng Chem Res* 2018;57(38):12942–50.
- [79] Chys M, van den Broek M, Vanslambrouck B, De Paepe M. Potential of zeotropic mixtures as working fluids in Organic Rankine Cycles. *Energy* 2012;44(1):623–32.
- [80] Lecompte S, Lemmens S, Huisseune H, van den Broek M, de Paepe M. Multi-Objective Thermo-Economic Optimization Strategy for ORCs Applied to Subcritical and Transcritical Cycles for Waste Heat Recovery. *Energies* 2015;8(4):2714–41.
- [81] Lampe M, de Servi C, Schilling J, Bardow A, Colonna P. Towards the integrated design of Organic Rankine Cycle power plants: A method for the simultaneous optimization of working fluid, thermodynamic cycle and turbine. *J Eng Gas Turbines Power* 2019;141(11):111009.
- [82] Mounier V, Mendoza LC, Schiffmann J. Thermo-economic optimization of an ORC driven heat pump based on small scale turbomachinery and comparison with absorption heat pumps. *International Journal of Refrigeration* 2017;81:96–110.
- [83] Bejan A, Tsatsaronis G, Moran MJ. Thermal design and optimization. A Wiley-Interscience publication; New York: Wiley; 1996. ISBN 0-471-58467-3.
- [84] Pierobon L, Nguyen TV, Larsen U, Haglind F, Elmegaard B. Multi-objective optimization of Organic Rankine Cycles for waste heat recovery: Application in an offshore platform. *Energy* 2013;58:538–49.
- [85] Chemical Engineering Plant Cost Index. 2017. URL: www.chemengonline.com; (accessed on May 17, 2017).
- [86] Astolfi M, Romano MC, Bombarda P, Macchi E. Binary ORC (Organic Rankine Cycles) power plants for the exploitation of medium–low temper-

- ature geothermal sources – Part B: Techno-economic optimization. *Energy* 2014;66:435–46.
- [87] Hall SG, Ahmad S, Smith R. Capital cost targets for heat exchanger networks comprising mixed materials of construction, pressure ratings and exchanger types. *Comput Chem Eng* 1990;14(3):319–35.
 - [88] Turton R, Bailie RC, Whiting WB, Shaeiwitz JA. Analysis, synthesis and design of chemical processes. Pearson Education International; 2008.
 - [89] Christensen P, Dysert LR, Bates J, Burton CDJ, Creese RC, Hollmann JK, et al. Cost estimate classification system—as applied in engineering, procurement, and construction for the process industries. AACE International Recommended Practice No 18R-97, TCM Framework: 73 – Cost Estimating and Budgeting 2005;.
 - [90] Gnielinski V. New equations for heat and mass transfer in the turbulent flow in pipes and channels. NASA STI/Recon Technical Report A 1975;75:8–16.
 - [91] Gnielinski V. Ein neues berechnungsverfahren für die wärmeübertragung im übergangsbereich zwischen laminarer und turbulenter rohrströmung. *Forschung im Ingenieurwesen* 1995;61(9):240–8.
 - [92] Kind M, Steiner D, Chawla JM, Schröder JJ, Saito Y, Auracher H, et al. H3 Flow Boiling. In: The Association of German Engineers , editor. VDI Heat Atlas. Berlin, Heidelberg: Springer Berlin Heidelberg. ISBN 978-3-540-77877-6; 2010, p. 793–902.
 - [93] Shah MM. A method for predicting heat transfer during boiling of mixtures in plain tubes. *Appl Therm Eng* 2015;89:812–21.
 - [94] Gungor KE, Winterton R. A general correlation for flow boiling in tubes and annuli. *Int J Heat Mass Transfer* 1986;29(3):351–8.

- [95] Dittus FW, Boelter L. Heat transfer in automobile radiators of the tubular type. *International Communications in Heat and Mass Transfer* 1985;12(1):3–22.
- [96] Bell J, Ghaly A. An approximate generalized design method for multicomponent/partial condensers. In: *AIChE Symp. Ser. Heat Transfer*; vol. 69. 1973, p. 72–9.
- [97] Cooper MG. Heat Flow Rates in Saturated Nucleate Pool Boiling-A Wide-Ranging Examination Using Reduced Properties. In: Hartnett JP, Irvine TF, editors. *Advances in heat transfer*; vol. 16 of Advances in Heat Transfer. Orlando and London: Academic Press. ISBN 9780120200160; 1984, p. 157–239.
- [98] Thome J, Shakir S. A new correlation for nucleate pool boiling of aqueous mixtures. *AIChE Symp Ser* 1987;83(257):41–51.
- [99] Numrich R, Müller J. J1 Filmwise Condensation of Pure Vapors. In: *The Association of German Engineers*, editor. *VDI Heat Atlas*. Berlin, Heidelberg: Springer Berlin Heidelberg. ISBN 978-3-540-77877-6; 2010, p. 903–18.
- [100] Burden RL, Faires JD. *Numerical analysis*. 9. ed., international ed. ed.; Belmont, Calif.: Brooks/Cole; 2011. ISBN 9780538733519.
- [101] Rayegan R, Tao Y. A procedure to select working fluids for Solar Organic Rankine Cycles (ORCs). *Renewable Energy* 2011;36(2):659–70.
- [102] Safarian S, Aramoun F. Energy and exergy assessments of modified Organic Rankine Cycles (ORCs). *Energy Reports* 2015;1:1–7.
- [103] Quoilin S, van Broek MD, Declaye S, Dewallef P, Lemort V. Techno-economic survey of Organic Rankine Cycle (ORC) systems. *Renew Sust Energ Rev* 2013;22:168–86.

- [104] Schwöbel JAH, Preißinger M, Brüggemann D, Klamt A. High-Throughput Screening of Working Fluids for the Organic Rankine Cycle (ORC) Based on Conductor-like Screening Model for Realistic Solvation (COSMO-RS) and Thermodynamic Process Simulations. *Ind Eng Chem Res* 2017;56(3):788–98.
- [105] Preißinger M, Schwöbel JA, Klamt A, Brüggemann D. Multi-criteria evaluation of several million working fluids for waste heat recovery by means of Organic Rankine Cycle in passenger cars and heavy-duty trucks. *Appl Energ* 2017;206:887–99.
- [106] Heberle F, Brüggemann D. Thermo-economic analysis of zeotropic mixtures and pure working fluids in Organic Rankine Cycles for waste heat recovery. *Energies* 2016;9(4):226.
- [107] Heberle F, Preißinger M, Brüggemann D. Zeotropic mixtures as working fluids in Organic Rankine Cycles for low-enthalpy geothermal resources. *Renew Energ* 2012;37(1):364–70.
- [108] Zebian H, Mitsos A. A double-pinch criterion for regenerative Rankine cycles. *Energy* 2012;40(1):258–70.
- [109] Bongartz D, Najman J, Sass S, Mitsos A. MAiNGO: McCormick based Algorithm for mixed integer Nonlinear Global Optimization. Tech. Rep.; Process Systems Engineering (AVT.SVT), RWTH Aachen University; 2018. URL: <http://permalink.avt.rwth-aachen.de/?id=729717>.
- [110] Bongartz D, Mitsos A. Deterministic global flowsheet optimization: Between equation-oriented and sequential-modular methods. *AIChE Journal* 2019;65(3):1022–34.